

Department of Civil & Construction Engineering

**An Analytical and Experimental Investigation of Polycal Wire Rope
Vibration Isolators for Industrial Equipment**


Ting Yuk Shyh

**This thesis is presented for the Degree of
Master of Philosophy (Civil Engineering)
of
Curtin University**

July 2018

Declaration

To the best of my knowledge and belief this thesis contains no material previously published by any other person except where due acknowledgment has been made. This thesis contains no material which has been accepted for the award of any other degree or diploma in any university.

Signature: 

Date: 10th July 2018

ACKNOWLEDGEMENTS

First of all, I would like to express my gratitude to my thesis supervisors, A/Prof. Dr. Muhammad Ekhlashur Rahman, Dr. Neamul Ahsan Noman Khandoker, Dr. Leblouba Moussa, Prof. Ir. Lau Hieng Ho and chairperson, Dr. Sumaiya Islam for their guidance and encouragement throughout my research work. It would be so much difficult without their help and comments.

Besides, I would like to show my gratitude to my senior, Mr. Balaji Palani Selvaraj for his guidance and valuable technical knowledge sharing on my work.

Also, thanks to Curtin University for providing tuition fee waiver and sophisticated lab equipment and MOHE, Malaysia for their financial support.

Lastly, I would like to thank my family and friends for their spiritual support and encouragement during my research period.

ABSTRACT

Vibration of an equipment or structure caused by the sources such as earthquake motion and operation of machinery can have destructive effect on it, particularly when the tolerable limit is exceeded. It can affect the functionality of the equipment and cause damage to the hosting structure. Therefore, vibration isolation system can be introduced to the equipment or structure to discontinue the transmission path of vibration and minimise its destructive effect before penetrating the hosting system. Polycal wire rope isolator (PWRI) is a type of discrete system that can isolate vibration effectively and is suitable for lightweight equipment and structure. The main advantage of PWRI is that it can be used and installed on the equipment in all three planes and in any orientation to isolate vibration. The PWRI is generally installed to separate the equipment from the base, supporting the whole equipment. Therefore, the isolation capability of PWRI can be examined by evaluating the stiffness and the damping characteristics of the isolator.

The study aims to enhance the current knowledge of and understanding on stiffness and damping characteristics of PWRIs. The main objective of this research work is to evaluate both analytical and experimental stiffnesses and experimental damping characteristics of PWRI in the vertical and lateral directions. Analytical models for vertical and lateral stiffnesses of PWRI were derived in this research work based on Castiglione's second theorem. Experimental work on the stiffnesses were also performed by conducting monotonic loading test to validate the analytical models. The analytical results agreed well with the experimental results for both vertical and lateral directions. Lastly, the damping characteristics of PWRI was studied through performing a series of cyclic loading tests.

Based on the study, it is shown that the wire rope diameter has more significant influence on the stiffness of PWRI than other geometrical properties. It was also found that the vertical stiffness of PWRI is two times greater than the lateral stiffness. Besides, experimental study was conducted for studying the damping characteristics. The results showed that the height-to-width ratio of PWRI affects the damping characteristics more significantly. It is found that increase in height-to-width ratio

resulted in more hardening effect of PWRI. Also, increase in height-to-width ratio of PWRI decreased the equivalent-damping ratio which actually dissipated more energy.

TABLE OF CONTENTS

ACKNOWLEDGEMENTS	II
ABSTRACT.....	III
NOTATIONS.....	VII
ABBREVIATION.....	IX
LIST OF FIGURES	X
LIST OF TABLES.....	XIII
1. INTRODUCTION	1
1.1. Vibration	1
1.2. Introduction of vibration isolation	2
1.3. Types of vibration isolation systems.....	4
1.4. Problem statement.....	5
1.5. Research gap	6
1.6. Research questions	6
1.7. Aim/objectives	6
1.8. Thesis outline	7
2. LITERATURE REVIEW	8
2.1. Introduction.....	8
2.2. Research work on nonlinear vibration isolators.....	8
2.2.1. Beams as nonlinear springs.....	8
2.2.2. Materials with nonlinear behaviour	10
2.2.3. Summary	11
2.3. Wire Rope for Vibration Isolation	12
2.3.1. Wire rope	12
2.3.2. Wire rope isolators	13
2.4. Damping behaviour of WRI under Cyclic Loading Condition.....	17
2.4.1. Hysteresis Loop Area and Energy loss ratio	18
2.4.2. Effective stiffness.....	19
2.5. Summary from literature review	20
3. STATIC STIFFNESS OF PWRI	21
3.1. Introduction.....	21
3.2. Methodology and scope	21
3.3. Application of Castigliano's Theorem.....	22
3.4. Geometry of the PWRI	22
3.5. Analytical model of stiffness of the PWRI	24

3.5.1.	Analytical model of Vertical Stiffness of the PWRI.....	25
3.5.2.	Analytical model of lateral stiffness (k_L)	28
3.6.	Experimental Setup	29
3.6.1.	Equipment	30
3.6.2.	Test specimens	30
3.6.3.	Fixture design.....	31
3.6.4.	Experimental procedure	31
3.7.	Results.....	32
3.8.	Parametric Analysis	34
3.8.1.	Influence of wire rope diameter	34
3.8.2.	Influence of radius of curvature of wire rope, width, and height on the PWRI ...	35
3.8.3.	Influence of the Number of wire rope strips	36
3.9.	Summary	37
4.	HYSTERESIS BEHAVIOUR OF PWRI	38
4.1.	Introduction.....	38
4.2.	Methodology	38
4.3.	Experimental setup.....	38
4.3.1.	Evaluation of Damping Characteristics	39
4.4.	Damping Characteristic of PWRI	40
4.4.1.	Hysteresis behaviour	40
4.3.2	Energy loss ratio.....	44
4.4.2.	Effective stiffness.....	48
4.4.3.	Equivalent Viscous Damping Ratio (EVDR)	53
4.5.	Influence of Loading frequency	57
4.6.	Influence of height-to-width ratio of PWRI.....	58
4.7.	Summary	62
5.	CONCLUSIONS AND RECOMMENDATIONS	63
5.1.	Introduction.....	63
5.1.1.	Objective 1	63
5.1.2.	Objective 2	64
5.1.3.	Objective 3	64
5.2.	Recommendation for future work	65
REFERENCES	66

NOTATIONS

A	: Height of the bevel of the top plate
B	: Width of the bevel of the bottom plate
D	: Diameter of wire rope
D_1	: Diameter of top plate
D_2	: Diameter of bottom plate
E	: Modulus of elasticity
E_d	: Area within the hysteresis loop
E_s	: Restored elastic energy
F	: Force or Load
H	: Height of the PWRI
I	: Moment of inertia
K_1	: Initial loading and initial unloading stiffness
K_2	: Final loading and final unloading stiffness
K_v	: Vertical stiffness of the PWRI
K_L	: Lateral stiffness of the PWRI
K_{eff}	: Effective Stiffness
M_o	: Indeterminate moment
M_1	: Moment in Sec. 1
N	: Number of wire rope strip
P	: Load on the entire PWRI
Q	: Shear Force
R	: radius of curvature of wire rope
T_1	: Thickness of the top plate
T_2	: Thickness of the bottom plate
U	: Strain Energy
W	: Width of the PWRI
X	: Displacement amplitude
x	: Coordinate in x-axis

- y : Coordinate in y-axis
 ζ_{eq} : Equivalent viscous damping ratio
 δ : Deflection

ABBREVIATION

ELR	: Energy Loss Ratio
EVDR	: Equivalent Viscous Damping Ratio
PWRI	: Polycal Wire Rope Isolator
SDOF	: Single Degree of Freedom
UTTM	: Universal Tensile Testing Machine
WRI	: Wire Rope Isolator

LIST OF FIGURES

Figure 1.1 Source, path and receiver components in the vibration system (Hunaidi, 2000)	2
Figure 1.2 Schematic of a SDOF system	3
Figure 1.3 Transmissibility-frequency ratio curve of SDOF system (Abolfathi, 2012)	3
Figure 1.4 Different types of Isolation System (Karnopp, 1995)	5
Figure 2.1 Euler spring (Winterflood, Barber, et al., 2002).....	9
Figure 2.2 Schematic illustration of the isolator with beam column (Platus, 1992)....	9
Figure 2.3 Lead-rubber elliptical leaf spring (Leblouba et al., 2015)	10
Figure 2.4 Wire rope components (Miller, 2004)	12
Figure 2.5 Application of Stockbridge damper (O. Barry et al., 2015)	13
Figure 2.6 (a) Polycal wire rope isolator; (b) helical wire rope isolator (DPFLEX, 2017a).....	14
Figure 2.7 Geometric characteristics (a) Helical WRI (b) Polycal WRI	15
Figure 2.8 Types of Loading Conditions (DPFLEX, 2017a).....	15
Figure 2.9 The double-linear retarding model (Weimin et al., 1997)	16
Figure 2.10 Hysteresis behaviours under cyclic loading (a) Lateral roll loading condition (b) Vertical loading condition (Demetriades et al., 1993)	18
Figure 2.11 Hysteresis Loop (Foss, 2006)	19
Figure 2.12 (a) Hysteresis loop area vs displacement amplitude (Y. Q. Ni et al., 1999) (b) Effective stiffness vs displacement amplitude (Y. Q. Ni et al., 1999).....	19
Figure 3.1 (a) Geometric properties of the PWRI; (b) Vertical and lateral loading on the PWRI.....	23
Figure 3.2 Free body diagram of a single wire rope strip	25
Figure 3.3 Variation of the flexural rigidity (EI) with a wire rope diameter (6 x 19 IWRC) (P. S. Balaji et al., 2016).....	27
Figure 3.4 Lateral loading on a wire rope strip	28
Figure 3.5 INSTRON Universal Tensile Testing Machine 5982.....	30
Figure 3.6 Fixtures used for the PWRI during loading test (a) Vertical fixtures (b) Lateral fixtures	31
Figure 3.7 The double-linear retarding model of the PWRI	32

Figure 3.8 The influence of wire rope diameter, D and number of wire rope strip, $N = 8$ on vertical and lateral stiffness, with a constant radius of curvature, $R=38\text{mm}$	35
Figure 3.9 Influence of the radius of curvature on vertical and lateral stiffness with 8 numbers of wire rope strips and 6.4mm diameter of wire rope	36
Figure 3.10 Influence of the number of wire rope strips on stiffness	37
Figure 4.1 Hysteresis behaviour of isolators in vertical direction (1mm).....	41
Figure 4.2 Hysteresis behaviour of isolators in vertical direction (2mm).....	41
Figure 4.3 Hysteresis behaviour of isolators in vertical direction (3mm).....	42
Figure 4.4 Hysteresis behaviour of isolators in Lateral Direction (1mm)	43
Figure 4.5 Hysteresis behaviour of isolators in Lateral Direction (2mm)	43
Figure 4.6 Hysteresis behaviour of isolators in Lateral Direction (3mm)	44
Figure 4.7 Energy Loss Ratio Diagram of Isolators (Vertical Direction).....	46
Figure 4.8 Energy Loss Ratio Diagram of Isolators (Lateral Direction)	48
Figure 4.9 Effective Stiffness vs Displacement Amplitude (Vertical Direction)	50
Figure 4.10 Normalized Effective Stiffness vs Displacement Amplitude (Vertical Direction)	51
Figure 4.11 Effective Stiffness vs Displacement Amplitude (Lateral Direction).....	53
Figure 4.12 Normalized Effective Stiffness vs Displacement Amplitude (Lateral Direction)	53
Figure 4.13 Equivalent Viscous Damping Ratio vs Displacement Amplitude (Vertical Direction)	55
Figure 4.14 Equivalent Viscous Damping Ratio vs Displacement Amplitude (Lateral Direction)	57
Figure 4.15 Rate Test for isolator 9 in tension/compression (wire rope diameter = 4.8mm)	58
Figure 4.16 Rate Test for isolator 9 in lateral mode (wire rope diameter = 4.8mm) .	58
Figure 4.17 Variation of Energy Loss Ratio with height-to-width ratio in vertical direction.....	59
Figure 4.18 Variation of Energy Loss Ratio with height-to-width ratio in lateral direction.....	60
Figure 4.19 Variation of Effective Stiffness with height-to-width ratio in vertical direction.....	60
Figure 4.20 Variation of Effective Stiffness with height-to-width ratio in lateral direction.....	61

Figure 4.21 Variation of Equivalent Viscous Damping Ratio with height-to-width ratio in vertical direction	61
Figure 4.22 Variation of Equivalent Viscous Damping Ratio with height-to-width ratio in lateral direction	62

LIST OF TABLES

Table 3.1 The geometrical properties of the PWRI	30
Table 3.2 Comparison between analytical and experimental vertical stiffness of the PWRI.....	33
Table 3.3 Comparison of analytical and experimental lateral stiffness results.....	34
Table 4.1 Experiment Data of Isolators from Hysteresis Curve (Vertical Direction)	44
Table 4.2 Experiment Data for ELR from Hysteresis Curve (Lateral Direction).....	47
Table 4.3 Experiment Data for Effective Stiffness from Hysteresis Curve (Vertical Direction)	49
Table 4.4 Experiment Data for Effective Stiffness from Hysteresis Curve (Lateral Direction)	52
Table 4.5 Experiment Data for Equivalent Viscous Damping Ratio from Hysteresis Curve (Vertical Direction)	54
Table 4.6 Experiment Data for Equivalent Viscous Damping Ratio from Hysteresis Curve (Lateral Direction).....	56

1. INTRODUCTION

1.1. Vibration

Vibration is a phenomenon where a rigid or elastic body forcefully oscillates or reciprocates from a state of equilibrium in a periodic motion when external force is applied. Vibration will be undesirable, if it exceeds the tolerable limit. Hence, vibration control is essential to reduce the damaging effects of vibrations to susceptible equipment. In order to mitigate the damages caused by vibration, it is necessary to design an effective vibration isolation system. Source, medium and receiver are the three main components of vibrations, shown in Figure 1.1 (Simmons, 2007). It is important to identify these components first before determining how to apply a vibration isolation system.

Vibration exists in many forms. Earthquakes, wind, ocean waves etc. are some of the natural causes of vibration. Whereas rotating or reciprocating machinery and the movement of heavy transport such as trailers, trucks and trains are all common sources of manmade vibration(s). Building components and equipment supports are examples of the path or medium transmitting vibration. The equipment or building which absorbs vibration is the receiver.

The function of a vibration control system is to interrupt the transmission path in such a way the vibrational energy encountered by the receiver is significantly reduced to a point the receiver can withstand the energy encountered without a change in the structural condition or functionality of the receiver. Vibration control systems can serve as path conditioners for the receiver, either by diverting a portion of the energy for each oscillation away from the receiver (as is the case of a tuned-mass damper), or by absorbing the said energy via damping mechanisms such as friction, viscous effects, or the induction of a magnetic field, whereby the energy produced by the vibrational source is converted into other forms such as heat, a change in the condition of a sacrificial material through wear and tear, an increase in kinetic energy of a damping fluid medium, the creation and destruction of magnetic flux, etc. (Klembczyk, 2009; Mallik, 1990)

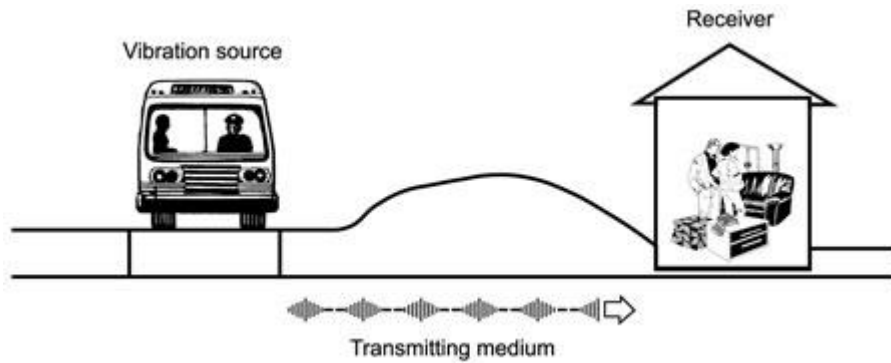


Figure 1.1 Source, medium and receiver components in the vibration system
(Hunaidi, 2000)

1.2. Introduction of vibration isolation

Vibration isolation is the act of reducing the oscillatory response of a receiver due to external sources of excitation such that the amplitude of response by the receiver is below damaging levels (Rivin, 2003). In the literature of vibration isolation, its usage is categorized under two primary cases. In the first case, the isolation system is used to reduce vibratory disturbances caused by heavy vibrating machinery. Regarding the second case, an isolation system is utilized to ensure the precision and accuracy of sensitive equipment is not affected by external vibrating sources. Concerning the two cases mentioned previously, Malik (1990) claimed both isolation systems work on similar principles. The system principle is based on a ‘single degree of freedom’ system (SDOF) (Den Hartog, 1985), shown in Figure 1.2. The isolating system depicted in Figure 1.2 shows the stiffness (K) and damping (C) of an isolator which supports an equipment’s mass (M). The magnitude of the stiffness and the equipment’s mass is used to calculate the natural frequency (ω_n) of an undamped SDOF system, as presented in Equation 1.1. In Figure 1.2, F_B refers to the harmonic force with forced frequency (ω) that excites the system while F refers to the force exerted on the equipment. The ratio of F to F_B is known as the transmissibility (T).

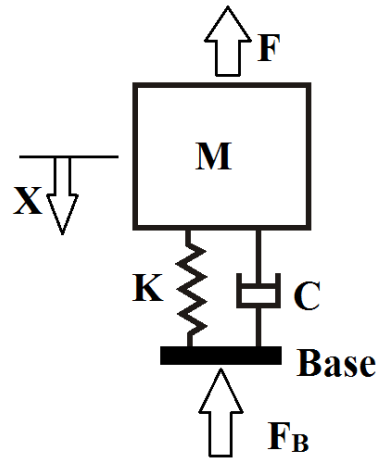


Figure 1.2 Schematic of a SDOF system

$$\omega_n = \sqrt{K/M} \text{ in rad/sec} \tag{1.1}$$

Figure 1.3 shows the transmissibility of SDOF with different damping ratios. A resonance condition happened at the peak of the transmissibility curve when the frequency ratio was one. Force exerted on the equipment is less than the external force when transmissibility of a system is less than one, which can be achieved by using an isolator. Isolation frequency is referred to as the frequency at the point where all the transmissibility curves cross at a frequency ratio of $\sqrt{2}$ (Abolfathi, 2012). Hence, more effective vibration isolation can be achieved if natural frequency is lower than the forced frequency. The acceptable transmissibility depends on the vibration sensitivity of the application, ranging from 3% to 10% (Simmons, 2007).

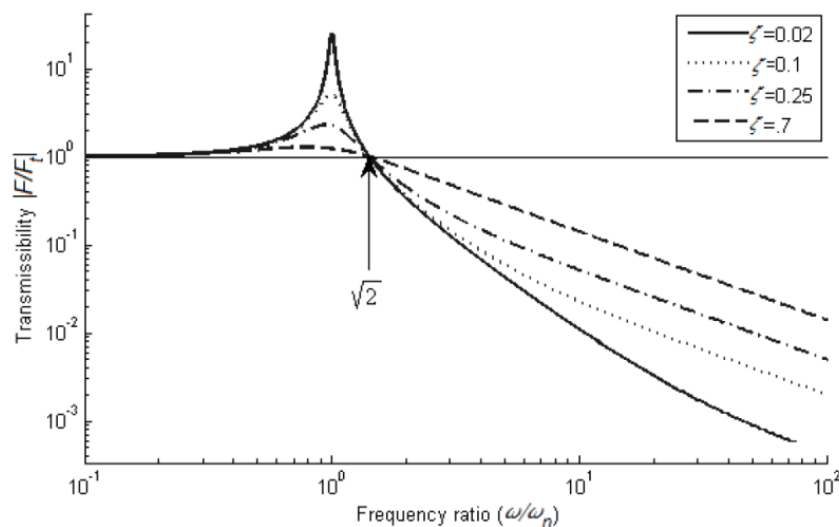


Figure 1.3 Transmissibility-frequency ratio curve of SDOF system (Abolfathi, 2012)

1.3. Types of vibration isolation systems

Vibration isolation systems can generally be classified into three types, active, semi-active and passive systems (Figure 1.4). Active vibration isolation systems have the highest performance in structural vibrational control among the three types (Hoque et al., 2010; Preumont, 2002; Tanaka & Kikushima, 1989). Semi-active isolation systems or adaptive-passive systems consists of a spring, damper and a feedback circuit. The feedback circuit contains an accelerometer, a signal processing device and an actuator such as the Magneto-rheological (MR) actuator (Dominguez et al., 2008). It has a relatively higher vibration control effectiveness than the passive isolation system since it can receive feedback from the accelerometer in real time and control the actuator to dissipate the energy accordingly (Dong et al., 2005; Preumont, 2002). However, a totally active system controls vibration using an actuator without a passive damper (Alanoly & Sankar, 1987; Karnaukhov & Tkachenko, 2011). The main disadvantages of the active and semi-active isolation systems are they require significant energy to operate, a high complexity in design, and accessories like accelerometers and signal processing devices, which can incur high manufacturing costs. Therefore, only very sensitive equipment which requires a high level of isolation need to employ active vibration isolation systems (Rivin, 2003).

Passive vibration isolation is the method of vibration reduction by utilizing passive media such as rubber isolators or spring isolators. It can be simplified as a spring with a stiffness coefficient (K), which represents elasticity of the system and a damper with a damping coefficient C , which dissipates energy (Figure 1.4(c)). Since the passive vibration isolation system has a simple design and is inexpensive, it has become the most common vibration isolation system (Rivin, 2003). This system can reduce the vibration effects from natural disasters and thus protect aging structures. Passive vibration isolation systems do not require any power supply in contrast with the other isolation systems. In addition, passive isolation devices can be easily maintained since the design is simple and not an integrated part of the protected structure (G. Li & Li, 2009).

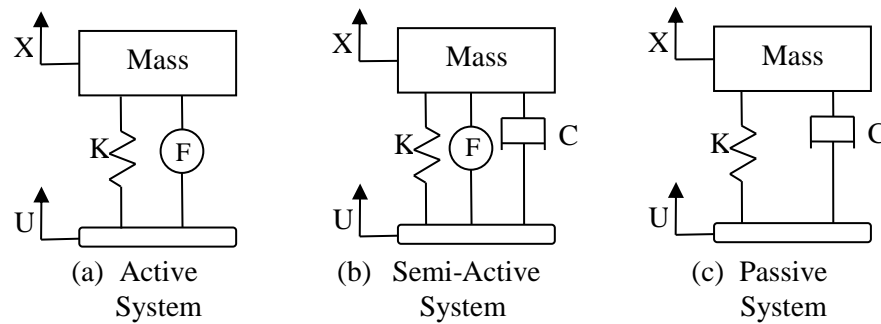


Figure 1.4 Different types of Isolation System (Karnopp, 1995)

1.4. Problem statement

The vibrations from sources such as an earthquake or due to operations of heavy machinery can affect the functionality and cause structural damage to structures and surrounding equipment. Hence, adding a discrete system to isolate the vibration from source becomes necessary. There are two major types of discrete systems employed for vibration isolation of equipment and structures: active and passive isolation systems. Active systems are very design intensive and require sensors and processors to provide realtime data to the isolator. In addition, it requires a large amount of power to operate. These necessary features of active isolation systems make it the most expensive isolation design. As a consequence of the expense and the large power requirement, active isolation systems are very uncommon in major industries. Passive vibration isolation, on the other hand, refers to vibration isolation by passive techniques such as rubber pads or mechanical springs. Different types of passive isolation devices are used and they can be broadly categorised as linear and non-linear isolators. However, linear possess a major drawback that it is useful only if the excitation frequencies are higher than the natural frequency of the isolator. Hence, linear isolators are limited to applications which have a moderate disturbance. Moreover, disturbance such as shock, impact load or random ground motion may contain a low-frequency component in their spectrum, hence, under these conditions, linear isolators leads to excessive deflection and in turn may cause over-stress and damage to the system. This drawback can be overcome by using non-linear isolators. Recently, PWRI a type of new passive isolator which, exhibits a non-linear behaviour, has become the subject of intensive study. Designing a proper isolation system requires a deep understanding of all parameters influencing its behaviour. Understanding the

behaviour of wire rope isolators allows us to construct a robust mathematical model that will calculate the vertical and lateral stiffness of PWRI.

1.5. Research gap

The study of the stiffness and the hysteresis behaviour of wire rope isolators (WRI) are important in the designing and selecting of vibration isolators to protect equipment. A few studies have been conducted to assess stiffness and the post elastic behaviour of helical WRIs (HWRI). However, there is no research on polycal WRIs (PWRI).

1.6. Research questions

The research questions are as follows:

- Can application of Castiglione's second theorem develop an effective mathematical model that can evaluate the vertical stiffness and lateral stiffness of PWRI subjected to experimental validation?
- How do the parameters (number of wire rope strips, diameter of the wire rope, width and height of the PWRI) affect the validity of the mathematical model?
- What is the damping characteristics of PWRI and how they are influenced under different loading condition?

1.7. Aim/objectives

This project aims to investigate stiffness and the damping characteristics of polycal wire rope isolators for industrial equipment.

The objectives of this project are as follow:

- I. To establish a mathematical model of the stiffness of polycal wire rope isolators in both vertical and lateral directions and validate with the monotonic loading test results.
- II. To investigate the damping characteristics of polycal wire rope isolators using cyclic loading conditions in both vertical and lateral directions.

- III. To determine the effect of the wire rope's diameter, width and height on the stiffness using parametric study.

1.8. Thesis outline

The outline of this thesis is summarized as below:

Chapter 2 summarizes previous research conducted on wire rope isolators and other non-linear isolators and reviews their characteristics and contributions.

Chapter 3 presents the mathematical models to calculate PWRI stiffness in vertical and lateral direction. The models are validated based on the study's results. A parametric study is carried out to study the effects of the PWRI's parameters on stiffness.

Chapter 4 discusses the investigation of the damping characteristics of the polycal wire rope isolator. The study's results obtained from the cyclic loading tests are used to calculate the damping characteristics.

Chapter 5 discusses the implications of this research, and recommendations for future work.

2. LITERATURE REVIEW

2.1. Introduction

This chapter provides the background of a nonlinear isolator, including the developments and reviews of their characteristics and performance over the years. The literature of nonlinear isolators in general was covered in this chapter which was then followed by the detailed review on the characterisation of wire rope isolators (WRI), emphasizing in stiffness and its hysteresis behaviour.

2.2. Research work on nonlinear vibration isolators

Nonlinear characteristic is indeed an important study for the development in nonlinear isolator. There are several studies on the literature of nonlinear isolators. Two types of isolators are reviewed in this research work due to its significant relevance to the WRI used in this study. First, the beams which work as nonlinear springs, and its stiffness is the main element of concern. Secondly, materials with nonlinear behaviour which their stiffness and damping properties are the main influencing factors in making selection.

2.2.1. Beams as nonlinear springs

The beam works as nonlinear spring since it has non-linear behaviour when encounter higher degree of bending (Abolfathi, 2012). It shows softening effect when under higher degree of bending and hence reducing natural frequency of the isolators which made of beams. The beams are normally able to load transversely or/and axially. Beam-column and Euler springs are discussed as below.

2.2.1.1. Euler springs

Euler springs is applying the concept of the column which loaded axially until it undergo buckling where it show nonlinear force displacement (Figure 2.1). Winterflood et al. (2002; 2002a) have used the Euler buckling principle as nonlinear springs. They have created a mathematical model of the stiffness of the spring and geometric characteristics is considered in the models (Winterflood et al., 2002). Davis

(2003) applied second order approximation on force-deflection relation for stiffness of vibration isolator that using buckled struts.

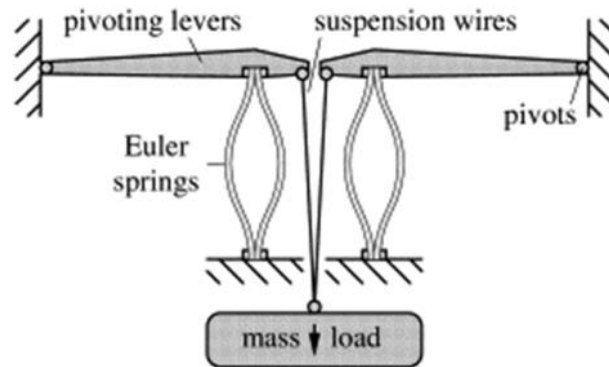


Figure 2.1 Euler spring (Winterflood et al., 2002)

2.2.1.2. Beam column

The development of beam column is based on the theory where force is applied transversely and axially since both loading shows non-linear force displacement. Figure 2.2 shows the schematic illustration of the beam column isolator. Platus (1992) has applied beam-column effect in his design and the isolators can be used for small and sensitive mechanical applications. Haberman (2007) has studied the force-displacement behaviour of similar isolator using experiments and mathematical modelling. While, Abolfathi (2012) has created the mathematical model of the static stiffness based on the concept of curved beam.

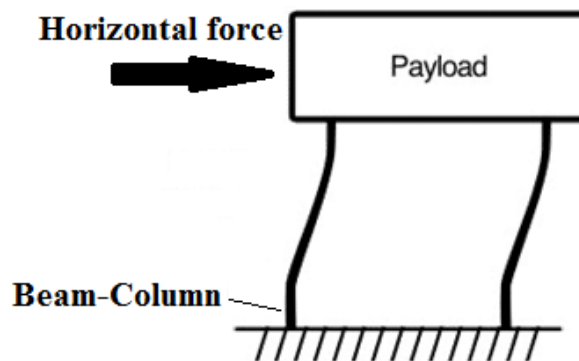


Figure 2.2 Schematic illustration of the isolator with beam column (Platus, 1992)

2.2.2. Materials with nonlinear behaviour

There are many types of materials such as composite, rubber and wire rope which behave non-linear of force-displacement. They consist of a spring element and a damping element which is able to dissipate energy. Rubber is one type of viscoelastic material which are widely used for vibration isolation. McCallion and Davies (1955) have carried out study of the influences of the temperature, amplitude and frequency of oscillation on the mechanical properties of rubber isolators under compression dynamic condition. They attempted to create mathematical expression of dynamic behaviour of rubber-like material. Shaska et al. (2007) discovered that rubber-like material has lower transmissibility compare to others linear isolators. Leblouba et al. (2015) have proved that improved damping and energy dissipation of the lead-rubber elliptical leaf spring are partly due to the incorporating of the rubber (Figure 2.3).

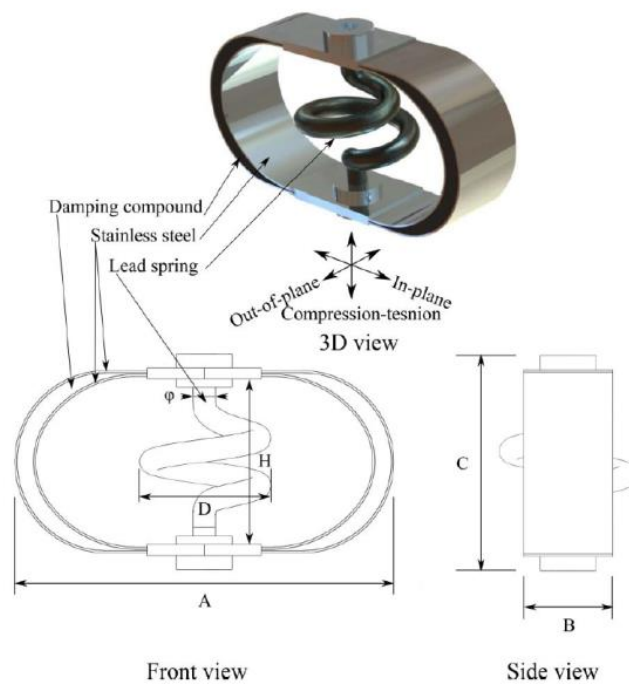


Figure 2.3 Lead-rubber elliptical leaf spring (Leblouba et al., 2015)

Besides, Mallick (1987) created a composite elliptic spring which is lighter in weight over steel spring while maintaining same damping performance. The demand of composite material in aerospace application has grown, since there is more convincing study of the composite behaviour published. Tse et al. (2002) have studied the stiffness of elliptical composite spring in lateral and vertical direction. They have developed

analytical and numerical model of the spring stiffness and validated with the experimental results.

Besides, there are few smart materials with nonlinear properties such as piezo-electrics, magneto-hydro-rheological fluids and electro-rheological fluids. The damping characteristics and stiffness of electro-rheological fluids can be altered using electric field, magneto-hydro-rheological fluids using magnetic field, and piezo-electrics using mechanical inputs (Ibrahim, 2008). Tandon et al. (1999) used starch powder and silica powder on colloidal suspensions to study electro-rheological fluids. They discovered that electric fields is able to control the damping properties and stiffness of the fluids. Guyomar et al. (2008) has conducted the experiment to study the vibration application by using piezo-electric materials. They proposed that excitation energy are converted into electric by using piezo-electric materials which later dissipates as heat by using electric shunt circuits. The smart materials have advantages in altering its damping characteristic and stiffness. However, their design are complex and it is required large operating power, which will increase in overall expenses. Hence, passive nonlinear isolator is preferred in this research.

2.2.3. Summary

The beams as nonlinear springs exhibit non-linearly in force deflection condition. However, the major disadvantage of the beams is that large deflection is required to encounter with low frequency of vibration (Abolfathi, 2012). They function well as a nonlinear spring but poor performance in damping especially during resonance. Moreover, vibration isolation designs using beams are currently only applied to micro mechanical field. Besides, materials with nonlinear characteristics such as piezo-electrics, magneto-hydro-rheological fluids and electro-rheological fluids have limitations with complex design and huge operating power. Rubber material are not robust when dealing with high temperature due to high damping condition or poor environment. Hence it can cause high manufacturing costs when special rubber materials are required. Therefore, development of nonlinear passive design take into consideration, wire rope isolators as vibration isolation which are passive and simple.

2.3. Wire Rope for Vibration Isolation

2.3.1. Wire rope

Wire ropes are commonly used in many application like lifting and hoisting in cranes and elevators, and holding for suspension bridges. The wire rope formed of twisted wire strands which the strands are formed of twisted thin metallic wires as shown in Figure 2.4. The core wire rope consists of either polypropylene, natural fibre or wire rope (G.A. Costello, 1997). According to Miller (2004), the core supports the strands and strands carry most of the load during normal loading and bending conditions.

Velinsky (1989; 1988, 2004) has conducted study on the wire rope characteristics with different type of configurations in term of design and mechanics aspects. He has stated the wire rope exhibits nonlinear behaviour in force-displacement. He has developed mathematical models and closed form solution to solve the non-linearity issue which caused by the complex interaction between the wires.

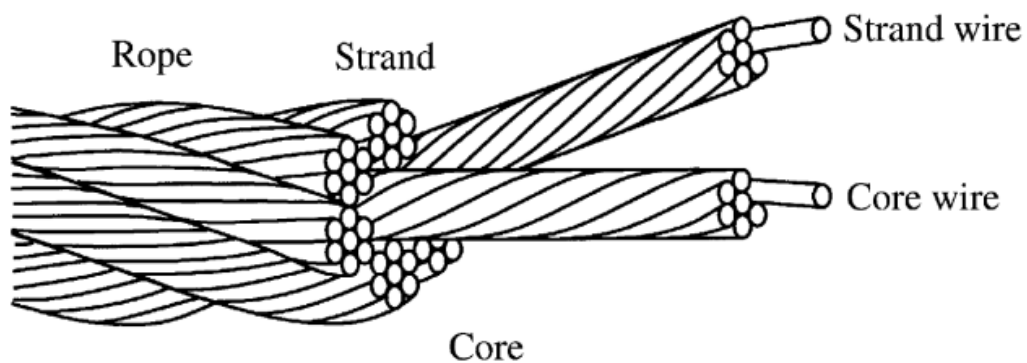


Figure 2.4 Wire rope components (Miller, 2004)

The wire rope has intrinsic frictional damping due to the frictional contact between wire strands. It performs well in most of the vibration isolation applications due to its nonlinear force-displacement and damping mechanism. Stockbridge damper is one of the wire rope application as vibration isolation in the past, shown in Figure 2.5. It is used to dampen wind induced vibrations on electric transmission lines or bridge cables (Oumar Barry et al., 2013)

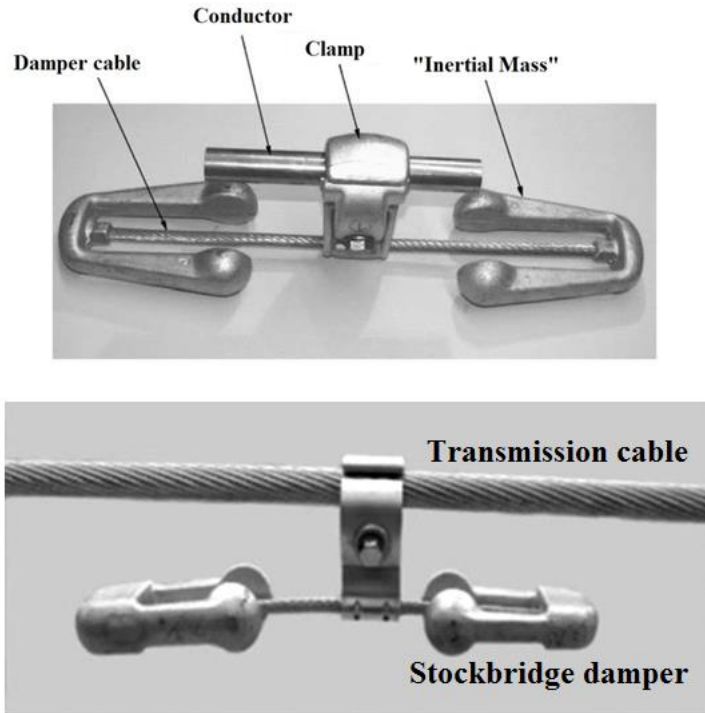


Figure 2.5 Application of Stockbridge damper (O. Barry et al., 2015)

2.3.2. Wire rope isolators

Constantinou et al. (1991) proposed one type of vibration isolator which made of wire rope, called wire rope isolator (WRI). The wire rope isolator (WRI) is a type of non-linear passive vibration isolator. Wire rope isolator consists of several wire ropes which are held in between two metal mounting plates which can be in spherical or helical shape, which is named polycal WRI (PWRI) Figure 2.6(a) and helical WRI Figure 2.6(b), respectively. Wire rope cables act as dampers because of their elastic properties from stranded wire rope. Moreover, sliding friction between intertwined cables, which dissipating energy as heat, provides further damping (M.L. Tinker, 1989; M. L. Tinker & Cutchins, 1992). Hence, it is considered as frictional type of damper. The wire rope is good in absorb impart energy and vibrational energy (Chungui et al., 2009; M. L. Tinker & Cutchins, 1992; Weimin et al., 1997). Figure 2.7 shows the geometric characteristics of WRIs.

The advantages of WRI are that it is durable, it requires low fabrication costs and it can be used in the extreme harsh environments, such as dusty, greasy and salty condition (DPFLEX, 2017b). It has a wide range of operating temperatures which are

from -100°C to $+250^{\circ}\text{C}$ (DPFLEX, 2017a). Due to the mechanical flexibility of the entire wire rope cables, WRI provides optimal isolation in all directions. WRI provides vertical and lateral loading conditions as shown in Figure 2.8. The helical isolators are mainly used for heavy duty equipment or machineries while PWRI are mainly used for light weight applications such as electronic devices.

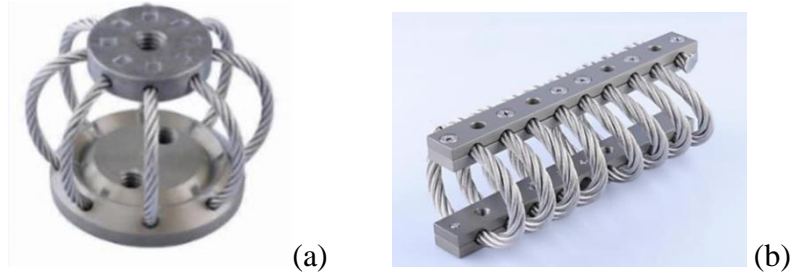


Figure 2.6 (a) Polycal wire rope isolator; (b) helical wire rope isolator (DPFLEX, 2017a)

WRI is widely used in many application since it is very effective in controlling both vibration and shock (M. L. Tinker & Cutchins, 1992). The application of WRI includes isolation of pipes in nuclear plant (Loziuk, 1988), cargo shipment (Chaudhuri & Kushwaha, 2008), sensitive electronic systems (Veprik & Babitsky, 2000), pipeline in aerospace systems and rocket engines (M. L. Tinker & Cutchins, 1992), light steel structures (Pagano & Strano, 2013), vibration isolation of industrial and defence equipment (Demetriades et al., 1993), noise and vibration control in military, naval and aerospace (Ledezma-Ramírez & Tapia-González, 2015) and in petroleum industries. Hence, detail study in the performance of WRI become necessary due to its significant and potential applications.

Stiffness and damping characteristic are the two main parameters which is used to define the performance of WRI. Wire rope spring design is the main component of stiffness of WRI which is the rigidity to resist the deformation due to external force. There is different stiffness under vertical and lateral loading conditions (P. S. Balaji et al., 2016; Palani S. Balaji et al., 2016). Damping characteristic of WRI is determined by its energy dissipation capability due to its intrinsic frictional damping. Thus, both stiffness and damping characteristic are the focus in the study in the following section. Literatures which related to stiffness and damping characteristic are discussed and reviewed.

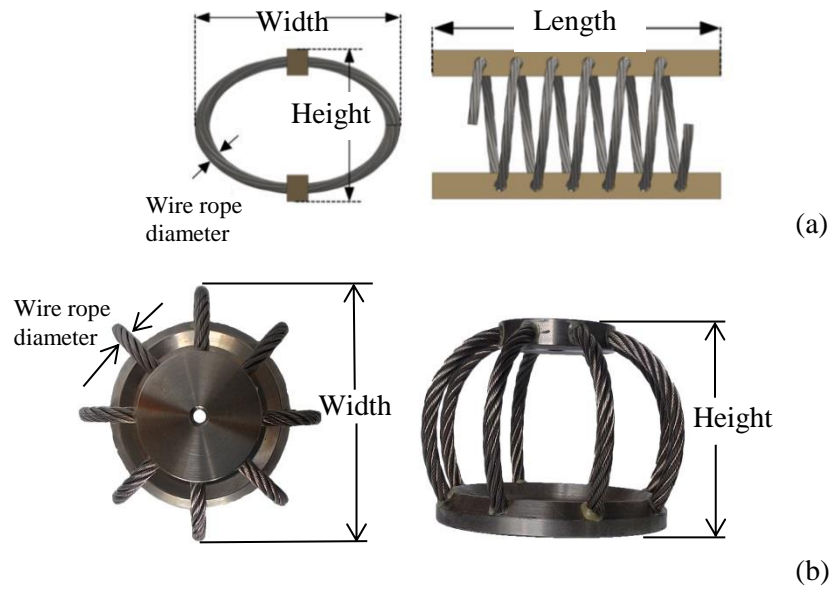


Figure 2.7 Geometric characteristics (a) Helical WRI (b) Polycal WRI

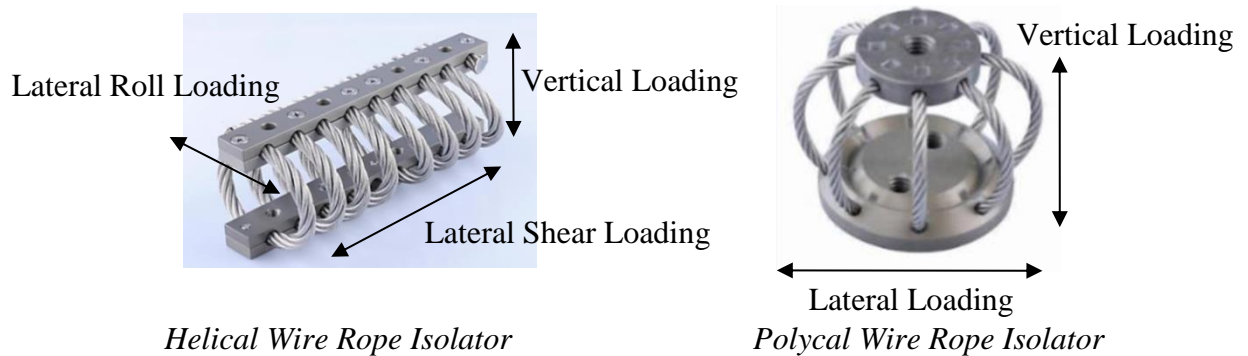


Figure 2.8 Types of Loading Conditions (DPFLEX, 2017a)

The static elastic stiffness is an important parameter in the selection of vibration isolator. Hence, the study of this behaviour is essential for monotonic loading. Manufacturers like ITT Inc. ("Wire rope Isolators," 2016) have carried out monotonic loading test for their products and determined static elastic stiffnesses from the load-displacement curves. However, due to expensive time-consuming experiments, it is essential to develop an analytical model for the static elastic stiffness. An ideal selection and design of WRI should employ analytical models which contain all the significant parameters.

Characteristic of stiffness can be determined through monotonic loading, which involves loading and unloading process in the experiment in this paper. During the loading process, the increase of the load on the isolator will lead the isolator to increase

in displacement. However, due to non-linear behaviour of the isolator, the gradient of the load-displacement curve or compression stiffness decrease, with an increase of the displacement. C. Weimin et al. (1997) explained the softening phenomenon is due to the certain degree of slip happens between wire rope strands and wire rope undergo a certain degree of twisting. He simplified the loading and unloading curve of the ring structure wire rope isolator into the double-linear retarding model in his paper. The stiffness is divided into two stiffness which are early stiffness, K_1 and later stiffness, K_2 , shown in Figure 2.9.

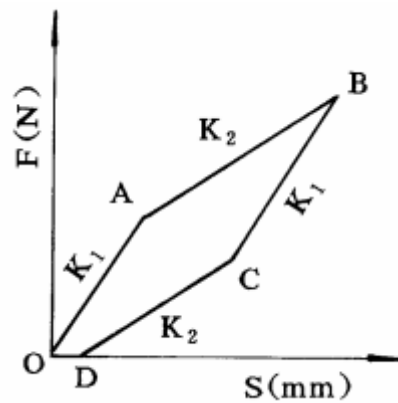


Figure 2.9 The double-linear retarding model (Weimin et al., 1997)

Tse et al. (2002) have developed analytical and numeral model of spring stiffnesses of composite circular springs in vertical compression, roll and shear and compared the results with monotonic loading experimental result while Balaji et al. (2016) has developed analytical model of vertical compression stiffness and roll stiffness of helical WRI and validated with monotonic loading experimental results. Ni et al. (1999) carried out an experimental study on static stiffness of helical WRI in roll, shear and tension-compression using monotonic loading test. Demetriades et al.(1993) showed that there has relation between stiffness with its wire rope properties and geometric characteristic. It is required to well understand the relation to produce a proper design of the PWRI. Tse and Balaji develop the analytical model using principle of potential energy and Castigliano's second theorem. The load is supported by bending the curved object has similarity in the concept between composite circular springs, helical WRI and PWRI. Due to similarity in the design, mathematical model of stiffness for PWRI can be established using similar methodology.

Castigliano's second theorem relates force-displacement with flexural rigidity (EI) of wire rope and geometric characteristics of the isolator. In order to simplified mathematical model of the flexural rigidity of a wire rope, Velinsky (1988, 2004) proposed several assumptions to make complicated interaction between wire strands simple. The flexural rigidity of all the wire strands is assumed as flexural rigidity of one wire rope.

Costello (1997) has applied similar assumption in his study of wire rope stress and strength distribution. His numerical model was well validated with experimental test results. Zhu, Meguid (2007) and Balaji et al. (2016) have conducted experiments on the wire rope in order to get flexural rigidity of the wire rope. The experiment method used is similar to the method which applied to test on the beams. As a short conclusion, due to similarity in WRI and composite circular springs designs, stiffness of PWRI can be calculated by using castigliano's theorem. Flexural rigidity of wire rope can be obtained analytically based on its properties.

2.4. Damping behaviour of WRI under Cyclic Loading Condition

The study of damping behaviour of WRI is to understand the damping characteristics of WRI under cyclic loading condition. Damping characteristics of WRI are determined by its energy dissipation capability. Existing studies of helical WRI are used as references in this research. Several researchers have carried out analysis of the hysteresis behaviour of helical WRI through experiments (Demetriades et al., 1993; Di Massa et al., 2013; M.L. Tinker, 1989; Y. Ni et al., 1999; Paolacci & Giannini, 2008; Tinker et al., 1992). From their results, it can be seen that WRI exhibits hysteresis curve under cyclic loading. The nature of the hysteresis curve shows the restoring force are direct related to both current and previous displacement (Ismail et al., 2009). The applied load also depends on the history of displacement (Demetriades et al., 1993; Wang et al., 2015b), which is referred as memory effect. Hysteresis is defined as a nature behaviour to dissipate energy and provide restoring force against displacement in mechanical and structural systems. (Ismail et al., 2009).

Tinker and Cutchin (1992) showed that the sliding friction among the individual wire strand in WRI cable caused the damping in the wire rope system. Study of Demetriades

et al. (1993) reveals that WRI shows the symmetric hysteresis behaviour under the lateral roll loading condition (Figure 2.10(a)). However, WRI shows the asymmetric hysteresis behaviour under the vertical loading Figure 2.10 (b) due to different stiffness in tension and in compression.

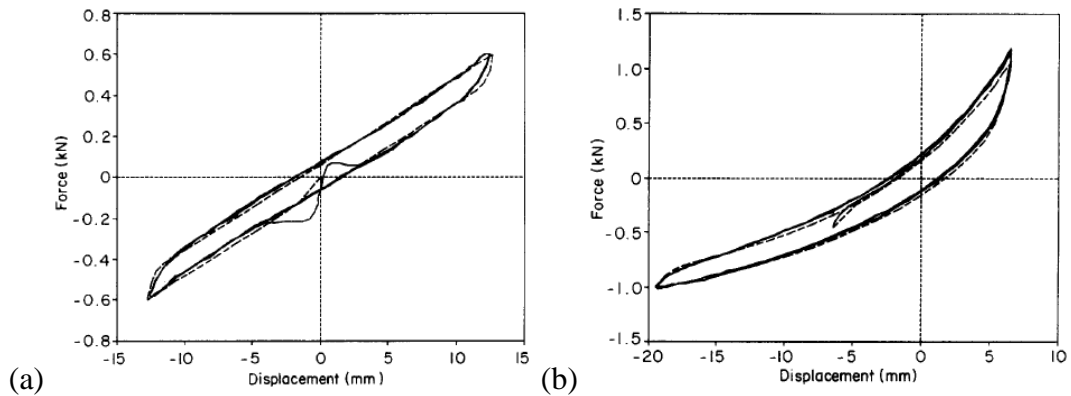


Figure 2.10 Hysteresis behaviours under cyclic loading (a) Lateral roll loading condition (b) Vertical loading condition (Demetriades et al., 1993)

The wire strands stick closer when tension load is applied. The frictional force increases due to the increased contact point. Thus, movement resistance is increased and hardening phenomenon occurred. Meanwhile, the wire strands separate further away from each other when compression load is applied. The frictional force is reduced due to the reduced surface of contact. Therefore, movement resistance is reduced and softening phenomenon happened. The hysteresis behaviour of the WRI is greatly influenced by different response characteristics like the direction of the applied force, the cable twist, the cable length, the numbers of strands, the diameter of wire rope (Demetriades et al., 1993). The area under the hysteresis curve represents the energy dissipated by WRI during cyclic loading condition (M.L. Tinker, 1989; Tinker et al., 1992).

2.4.1. Hysteresis Loop Area and Energy loss ratio

Foss (2006) explained hysteresis curve using hysteresis loop area, shown in Figure 2.11. The dissipated energy during one complete cyclic loading represented by the area within the yellow shape. Meanwhile, the maximum potential energy for load and displacement is represented by the area within the green circle. An increase in

displacement amplitude will increase the hysteresis loop area, as shown in Figure 2.12(a) (Y. Q. Ni et al., 1999).

Energy loss ratio (ELR) is one of the damping characteristic of WRI that evaluate the effectiveness of WRIs. ELR is defined as the amount of dissipated energy which caused by sliding friction between wire strands with reference to viscous damping (Balaji et al., 2015). Foss (2006) reported that greater values of ELR show greater damping capabilities of WRI.

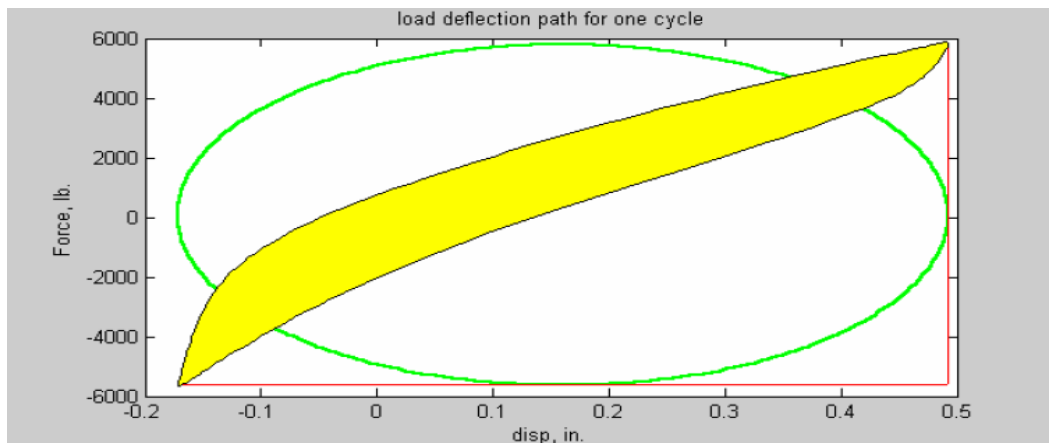


Figure 2.11 Hysteresis Loop (Foss, 2006)

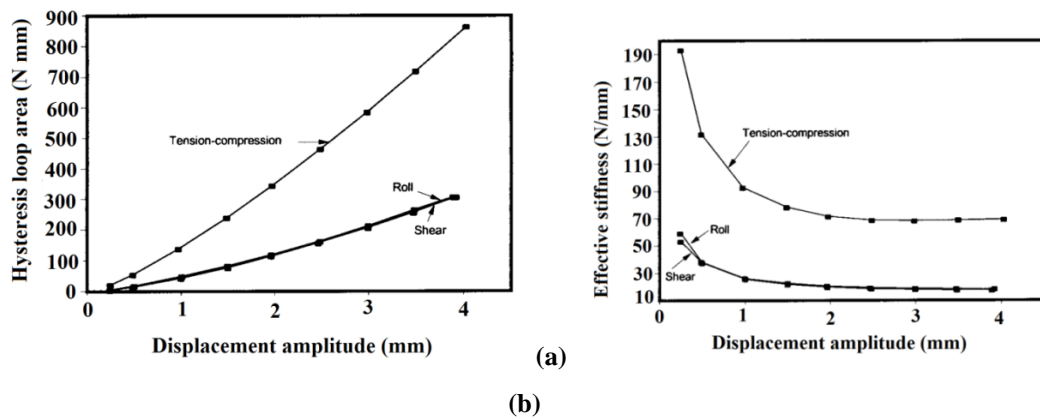


Figure 2.12 (a) Hysteresis loop area vs displacement amplitude (Y. Q. Ni et al., 1999) (b) Effective stiffness vs displacement amplitude (Y. Q. Ni et al., 1999)

2.4.2. Effective stiffness

Effective stiffness (K_{eff}) of WRI is the ratio of the largest and smallest changes of forces to the largest and smallest changes of displacement amplitudes (Balaji et al., 2015). The effective stiffness varies and one complete hysteresis loop is taken for

calculation, which the hysteresis loop requires static loading experimentation. Wang et al. (2015a) experimentally investigated the effect of amplitude on the effective stiffness (Figure 2.12b). They observed that the effective stiffness decreased as the displacement amplitude increased.

2.5. Summary from literature review

Systems which exhibit non-linearity were frequently prescribed for application in vibration isolation systems. In most researches concerning the use of non-linearity in vibration isolation systems, the non-linear stiffness characteristics were analysed experimentally. Besides, mathematical models were developed by analysis its deflection mechanism of the non-linear system which related to force and displacement. Static stiffness has emerged as an important specification for the selection of PWRI suitable for various practical applications. However, research on the static stiffness parameters has been mostly restricted to WRI. It is worthwhile to note that there is a similarity between PWRI and WRI, Hence the utilization of Castigliano's second theorem in PWRI stiffness model is deemed appropriate. In order to make ease of design and selection of PWRI, it is required a well-defined mathematical model which include all the significant parameters. Meanwhile, it is important to understand how the significant parameters effect the stiffness. Damping of the wire rope isolator is caused by the frictional sliding contact between wire strands which cause the PWRI to exhibit hysteresis behaviour. Thus, damping characteristic can be obtained through its hysteresis behaviour. There is very limited of significant research on damping characteristics of PWRI. Hence, it is required for investigation of the damping characteristics of PWRI to enhance the understanding of its performance for different application.

3. STATIC STIFFNESS OF PWRI

3.1. Introduction

This chapter presents the analytical models developed for both vertical and lateral stiffness of PWRI. The vertical compressive and lateral stiffness analytical models were developed based on Castigliano's second theorem. The models were validated using the monotonic loading tests in the respective directions. Finally, a parametric study was carried out to investigate the influence of the width, height, and diameter of the wire rope as well as the number of wire rope strips had on the vertical compressive stiffness and lateral stiffness of WRIs.

3.2. Methodology and scope

The methodology of derivation and the validation of analytical models are discussed in this section. A similar method used for deriving the mathematical model of WRI stiffness was used to derive the mathematical model of the PWRI stiffness which involved deflection of the wire rope. The analytical models of the vertical and lateral stiffness were derived from Castigliano's theorem, which has established the relationship between stiffness and geometric properties. These developed models can be useful in designing the PWRI. An experiment was carried out to determine the stiffness of the isolators with various geometrical properties through vertical and lateral loading. These experimental results were used to validate the mathematical model of stiffness. Deriving the analytical stiffness of the PWRI is challenging due to the nonlinear F-D characteristic. Currently in industries (DPFLEX, 2017b), stiffness of PWRIs are taken at small displacement from a selection of PWRIs. C. Weimin et al. (1997) has defined stiffness of a ring structure wire rope isolator using monotonic loading and unloading. Hence, monotonic loading and unloading with a small displacement was used to determine the stiffness in this work.

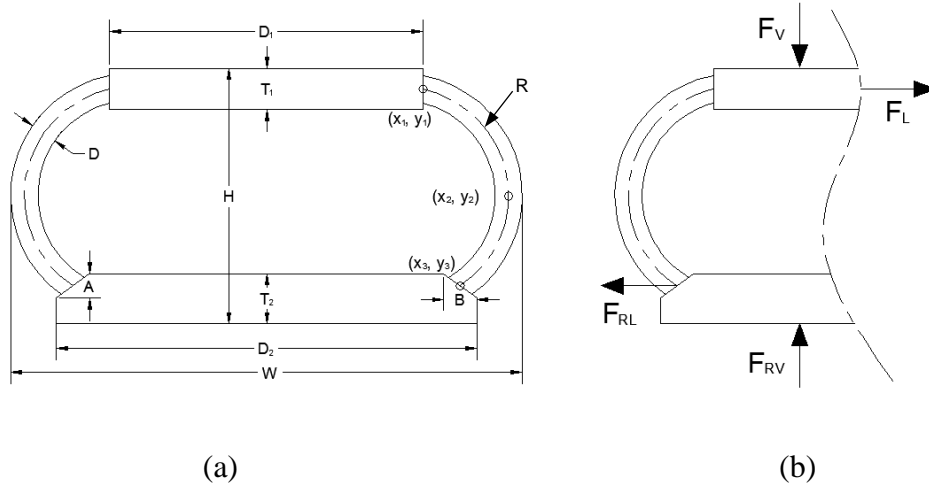
3.3. Application of Castigliano's Theorem

It is crucial to analysis the relationship between the applied force and the displacement in order to acquire the mathematical model for vertical and lateral stiffness of PWRI. When the WRI is acted upon by an external excitation, it displaces and when the excitation is removed, it returns to its initial position. The excitation energy is absorbed by the wire strands of the PWRI through friction, during displacement of the PWRI. Hence, the mechanical properties and shape of the PWRI is considered an important factor for developing the mathematical model. Displacement and strain energy are analysed through Castigliano's second theorem, which states *“when forces act on an elastic system subject to small displacements, the displacement corresponding to any force, in the direction of the force, is equal to the partial derivative of the total strain energy with respect to that force”* (Shigley, 2008). In order to simplify the analytical model, the following assumptions have been made.

1. The wire rope is treated as a solid bar with a uniform cross section;
2. Homogeneous and isotropic material properties of the wire rope are considered;
3. The load resistance of the metal mounting plates are neglected;
4. The vertical and lateral loading of the PWRI is quasistatic;
5. The PWRI is firmly fixed to the Universal Tensile Testing Machine

3.4. Geometry of the PWRI

In order to simplify the calculation in the development of the modelling, a single strip (Figure 3.1(b)) sustains vertical and lateral loads. Figure 3.1(a) shows geometrical properties of the PWRI, which is represented by nomenclature. The radius of curvature of the wire rope, R can be determined by identifying 3 points of coordinate along the wire rope. The first point of the wire rope (x_1, y_1) is represented as reference point $(0, 0)$, which is located at the point that connects to the top plate. The second point (x_2, y_2) is located in the middle of the wire rope and the third point, (x_3, y_3) is located at the endpoint that connects to the bottom plate.



A=Height of the bevel of the top plate; B=Width of the bevel of the bottom plate; D=Diameter of wire rope; D_1 =Diameter of top plate; D_2 =Diameter of bottom plate; F_L =Lateral load; F_v =Vertical load; F_{RL} =Lateral reaction force; F_{RV} =Vertical reaction force; H=Height of the PWRI; R=Radius of curvature of the wire rope; T_1 =Thickness of the top plate; T_2 =Thickness of the bottom plate; W=Width of the PWRI

Figure 3.1 (a) Geometric properties of the PWRI; (b) Free body diagram with vertical and lateral loading on the PWRI

Equations 3.1a – 3.1d are used to obtain x_2 , y_2 , x_3 and y_3

$$x_2 = \frac{1}{2}(W - D_1) - \frac{1}{2}D \quad (3.1a)$$

$$y_2 = \frac{1}{2}H - \frac{1}{2}T_1 \quad (3.1b)$$

$$x_3 = \frac{1}{2}(D_2 - D_1) - \frac{1}{2}B \quad (3.1c)$$

$$y_3 = H - \frac{1}{2}T_1 - T_2 + \frac{1}{2}A \quad (3.1d)$$

The substitution of x_1 , y_1 , x_2 , y_2 , x_3 and y_3 , into the Equation of the Circle (Equation 3.2a). By solving the three simultaneous equations, R can be obtained.

$$(x-h)^2 + (y-k)^2 = R^2 \quad (3.2a)$$

$$R = \left(\frac{\left((H - 2T_2 + A) \left(\left(\frac{1}{2}(W - D_1) - \frac{1}{2}D \right)^2 + \left(\frac{1}{2}H - \frac{1}{2}T_1 \right)^2 \right) - (H - T_1) \left(\left(\frac{1}{2}(D_2 - D_1) - \frac{1}{2}B \right)^2 - \left(\frac{1}{2}(W - D_1) - \frac{1}{2}D \right)^2 + \left(H - \frac{1}{2}T_1 - T_2 + \frac{1}{2}A \right)^2 - \left(\frac{1}{2}H - \frac{1}{2}T_1 \right)^2 \right) \right)}{(H - 2T_2 + A)(W - D_1) - D - (H - T_1)(D_2 - W - B + D)} \right)^2 + \left(\frac{\left((D_2 - D_1) - B \right) \left(\left(\frac{1}{2}(W - D_1) - \frac{1}{2}D \right)^2 + \left(\frac{1}{2}H - \frac{1}{2}T_1 \right)^2 \right) - ((W - D_1) - D) \left(\left(\frac{1}{2}(D_2 - D_1) - \frac{1}{2}B \right)^2 + \left(H - \frac{1}{2}T_1 - T_2 + \frac{1}{2}A \right)^2 \right)}{(H - T_1)(D_2 - D_1) - B - ((W - D_1) - D)(2H - T_1 - 2T_2 + A)} \right)^2 \right)^{\frac{1}{2}} \quad (3.2b)$$

Simplifying,

$$R = \left(\left(\frac{f(1)(f(2)^2 + f(3)^2) - 2f(3)(f(4)^2 - f(2)^2 + f(5)^2 - f(3)^2)}{f(1) \times 2f(2) - 2f(3) \times f(6)} \right)^2 + \left(\frac{2f(4)(f(2)^2 + f(3)^2) - 2f(2)(f(4)^2 + f(5)^2)}{2f(3) \times 2f(4) - 2f(2) \times 2f(5)} \right)^2 \right)^{\frac{1}{2}} \quad (3.2c)$$

in which

$$f(1) = H - 2T_2 + A \quad (3.2d)$$

$$f(2) = \frac{1}{2}(W - D_1) - \frac{1}{2}D \quad (3.2e)$$

$$f(3) = \frac{1}{2}H - \frac{1}{2}T_1 \quad (3.2f)$$

$$f(4) = \frac{1}{2}(D_2 - D_1) - \frac{1}{2}B \quad (3.2g)$$

$$f(5) = H - \frac{1}{2}T_1 - T_2 + \frac{1}{2}A \quad (3.2h)$$

$$f(6) = D_2 - W - B + D \quad (3.2i)$$

3.5. Analytical model of stiffness of the PWRI

Castigliano's theorem is often used to solve a problem like the deflection of a curved bar (Shigley, 2008). There are two equal and opposite forces, F_V acting on the top and bottom of the PWRI on a single strip of wire rope under compressive loading, and F_L

acting at a side way force under lateral loading (Figure 3.1(b)). $F=P/N$ where N represents the number of wire rope strips and P represents the total force on the PWRI. There is only one wire rope strip considered due to the equal load on each wire rope.

3.5.1. Analytical model of Vertical Stiffness of the PWRI

Figure 3.2 shows the free body diagram of a single wire rope strip. The boundary limit for the wire rope strip is 0 to $3\pi/4$. The shear stress at the cross section is omitted since the cross section of the PWRI is relatively small compared to its radius of curvature. Castigliano's theorem is used to determine the statically indeterminate of the bending moment M_0 .

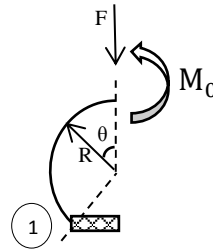


Figure 3.2 Free body diagram of a single wire rope strip

Due to the symmetrical geometry of the PWRI, its cross section remains fixed when the wire rope is being bent. Hence, M_0 will not cause any displacement, which is:

$$\frac{dU}{dM_0} = 0 \quad (3.3)$$

where U is the strain energy of a wire rope strip. The wire rope strip is in the form of a circular arc which can be considered the radius of curvature. Hence, Equation 3.3 is written as:

$$\frac{1}{EI} \left(\int_0^{\frac{3}{4}\pi} M_1 \frac{dM_1}{dM_0} R d\theta \right) = 0 \quad (3.4)$$

The bending moment of the full wire rope, M_1 is presented as:

$$M_1 = F(R \sin \theta) - M_0 \quad (3.5)$$

And

$$\frac{dM_1}{dM_o} = -1 \quad (3.6)$$

By substituting Equations 3.5 - 3.6 into Equation 3.4 and thus forming Equation 3.7:

$$\frac{1}{EI} \left(\int_0^{\frac{3}{4}\pi} (F(R \sin \theta) - M_o)(-1)R d\theta \right) = 0 \quad (3.7)$$

By solving Equation 3.7 for the statically indeterminate moment M_o , the following equation is given:

$$M_o = \frac{(2^{\frac{3}{2}} + 4)FR}{3\pi} \quad (3.8)$$

The total strain energy of the wire rope is described as:

$$U = \frac{1}{2EI} \times \left(\int_0^{\frac{3}{4}\pi} M_1^2 R d\theta \right) \quad (3.9)$$

By using Castigliano's theorem, we can obtain the deflection equation due to the applied load F described as:

$$\delta = \frac{dU}{dF} = \frac{1}{EI} \left(\int_0^{\frac{3}{4}\pi} M_1 \frac{dM_1}{dF} R d\theta \right) \quad (3.10)$$

Substituting Equation 3.5 into Equation 3.10 will result in:

$$\delta = \frac{F \left((9\pi^2 + 6\pi - 2^{\frac{11}{2}} - 48) \times R^3 \right)}{24\pi EI} \quad (3.11)$$

Lastly, the vertical stiffness (K_v) of the entire WRI is determined by the equation below:

$$\begin{aligned} K_v &= \frac{dP}{d\delta} \\ &= N \times \frac{24\pi EI}{(9\pi^2 + 6\pi - 2^{\frac{11}{2}} - 48) \times R^3} \end{aligned} \quad (3.12)$$

The flexural rigidity, EI which is used in the Equation 3.12, represents the resistance offered by the wire rope during bending, in which E is elastic stiffness and I is the moment of inertia. Few researchers have assumed the flexural rigidity of the wire rope as the total flexural rigidity of each wire strand, which can be modelled after a slender rod, with the addition of several dimensionless parameters to generalise the interaction between wire strands (George A Costello & Butson, 1982; Steven A Velinsky, 1988). Meanwhile, some researchers have proposed the analytical model of the properties and behaviour which assumes the cable as a solid rod (Huang & Vinogradov, 1994; Huang & Vinogradov, 1996a, 1996b; X. Li et al., 2014) and/or a cylinder (Hobbs & Raof, 1984; M Raof, 1991; Mohammed Raof, 1996; Mohammed Raof & Davies, 2006). Numerical studies have been carried out (Chiang, 1996; Jiang et al., 1999; Stanova et al., 2011a, 2011b) due to the complexity of developing an accurate analytical model. However, the disadvantage of the numerical studies is they are time-consuming for the simulation tests due to the large amount of data to simulate. These analytical and numerical models consider the axial tensile loading for single, straight and multi-strand wire ropes. These models have only described the behaviour of the ideal wire rope. In order to improve accuracy in the flexural rigidity of the actual wire rope, a transverse bending test has been carried out by Balaji et al. (2016). Since the same type of wire rope are used which is a 6 x 19 stainless steel Independent Wire Rope Core (IWRC), the flexural rigidity equation shown in Figure 3.3 is used in the present study.

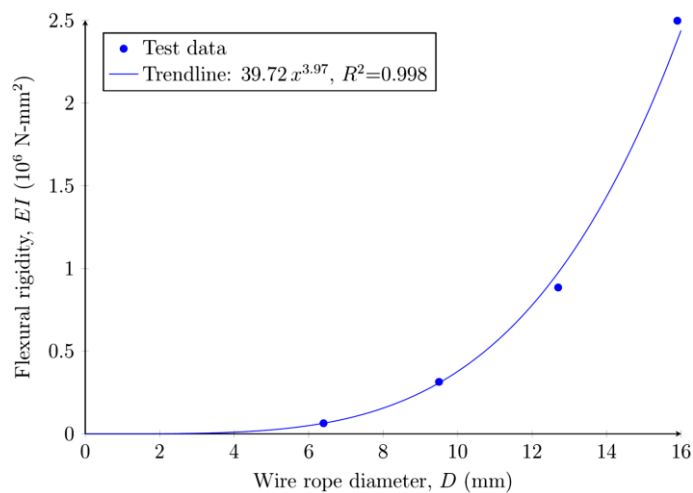


Figure 3.3 Variation of the flexural rigidity (EI) with a wire rope diameter (6 x 19 IWRC) (P. S. Balaji et al., 2016)

3.5.2. Analytical model of lateral stiffness (k_L)

A wire rope strip is considered in the development of the mathematical model and was subjected to a lateral load which shown in Figure 3.4. The wire rope strip boundary limits are from 0 to $3\pi/4$. The PWRI is fixed at the base and a load is created in a lateral direction. The wire rope strip is subjected to an indeterminate shear force and force F . However, the principle of least work (P. C. Tse et al., 2002) has been shown to eliminate the indeterminate bending moment.

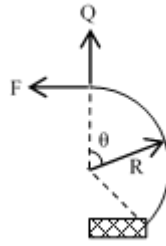


Figure 3.4 Lateral loading on a wire rope strip

The strain energy (U) of the wire rope strip is presented as:

$$U = \int_0^{\frac{3}{4}\pi} \frac{1}{2EI} M^2 R d\theta \quad (3.13)$$

Where M is the moment and is given by:

$$M = Q(R \sin \theta) - F(R - R \cos \theta); 0 \leq \theta \leq \frac{3}{4}\pi \quad (3.14)$$

Castigliano's theorem is used to define the indeterminate shear force Q . During the bending of the wire rope, its cross-section does not rotate since it is symmetrical as shown in Figure 3.4. Thus, the displacement is zero due to the shear force Q , given as:

$$\frac{dU}{dQ} = 0, \quad (3.15)$$

$$\frac{R^3}{16EI} [4Q + 6\pi Q - F(8\sqrt{2} + 12)] = 0$$

Upon solving Equation 3.15, the equation below can be applied to calculate the indeterminate shear force:

$$Q = \frac{F(8\sqrt{2} + 12)}{6\pi + 4} \quad (3.16)$$

Hence, the calculation of total strain energy stored in the one wire rope strip is:

$$\begin{aligned}
 U &= \int_0^{\frac{3}{4}\pi} \frac{R}{2EI} [Q(R \sin \theta) - F(R - R \cos \theta)]^2 d\theta \\
 &= \frac{R^3}{16EI} \left[9\pi F^2 - F^2(8\sqrt{2} + 2) + 3\pi Q^2 + 2Q^2 - FQ(8\sqrt{2} + 12) \right] \\
 &= - \frac{3F^2 R^3 \left(\frac{64\sqrt{2}}{3} - 9\pi^2 + \pi(8\sqrt{2} - 4) + 24 \right)}{16EI(3\pi + 2)} \\
 U &= \frac{F^2}{16} \left(\frac{R^3(-64\sqrt{2} + 27\pi^2 - 3\pi(8\sqrt{2} - 4) - 72)}{EI(3\pi + 2)} \right) \quad (3.17)
 \end{aligned}$$

The deflection of one wire rope strip due to the lateral load can be determined from the strain energy by utilizing Castigliano's theorem which is:

$$\delta_L = \frac{dU}{dF} \quad (3.18)$$

From Equation 3.17, the deflection of a single wire rope strip by the applied load F can be derived as:

$$\delta_L = \frac{F}{8} \left(\frac{R^3(-64\sqrt{2} + 27\pi^2 - 3\pi(8\sqrt{2} - 4) - 72)}{EI(3\pi + 2)} \right) \quad (3.19)$$

The load-displacement relationship of one wire rope strip is represented by Equation 3.19 with an assumption of small displacement amplitudes. Lastly, the lateral stiffness, k_L , for the entire PWRI is computed as:

$$K_L = N \times \frac{F}{\delta} = \frac{8EI(3\pi + 2)}{R^3(-64\sqrt{2} + 27\pi^2 - 3\pi(8\sqrt{2} - 4) - 72)} \quad (3.20)$$

3.6. Experimental Setup

A detailed experimental setup is shown in this section including the equipment, test specimens, fixtures design, and the experimental procedure.

3.6.1. Equipment

The monotonic loading experiment was carried out in-house using the INSTRON Universal Tensile Testing Machine (UTTM) (Figure 3.5). It is able to provide a maximum load of 100kN to the specimens. The testing machine sent the data to the Bluehill software and was then processed and displayed as a graph. The raw data was saved in the form of a graph in a PDF format as well as in an excel file. Several parameters such as loading speed, displacement and processes must be set properly into the Bluehill software before running the UTTM.

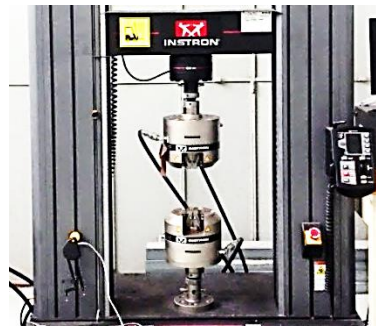


Figure 3.5 INSTRON Universal Tensile Testing Machine 5982

3.6.2. Test specimens

There were ten isolators which were tested in the present study. Each isolator has its unique geometrical properties such as height, width and wire rope diameter which is shown in Table 3.1. All of the isolators consist of a 6 x 19 stainless steel Independent Wire Rope Core (IWRC) wire rope. All wire ropes were held in a circular arrangement for the PWRI which are symmetric in vertical axis. The isolators are manufactured by Wuxi Hongyuan Devflex Co. Ltd. All the value shown in the Table 3.1 are the default parameters of PWRI from the manufacturer.

Table 3.1 The geometrical properties of the PWRI

No	Model	N	D (mm)	W (mm)	H (mm)	D_1 (mm)	D_2 (mm)	A (mm)	B (mm)	T_1 (mm)	T_2 (mm)
1	GGQ 1.0-37	8	2.5	76	37	52	70	5	5	7	10
2	GGQ 0.9-47	8	2.5	77	47	38	70	5	5	7	10
3	GGQ 0.55-56	8	2.5	80	56	26	70	5	5	7	10
4	GGQ 1.0-57	8	3.2	91	57	38	76	5	5	7	10

5	GGQ 1.7-71	8	3.2	96	71	26	76	5	5	7	10
6	GGQ 17-45	8	4.8	110	45	76	102	6	6	8	12
7	GGQ 15-62	8	4.8	113	62	64	102	6	6	8	12
8	GGQ 14-77	8	4.8	121	77	52	102	6	6	8	12
9	GGQ 29-71	8	6.4	120	71	64	102	6	6	10	12
10	GGQ 23-76	8	6.4	120	76	52	102	6	6	10	12

3.6.3. Fixture design

In the present experiment, the fixtures were designed to hold the isolator so it can only move in a vertical direction as shown in Figure 3.6(a), or in a lateral direction as shown in Figure 3.6(b). Each end of the PWRI was bolted tightly onto each fixture before being clamped to the machine.

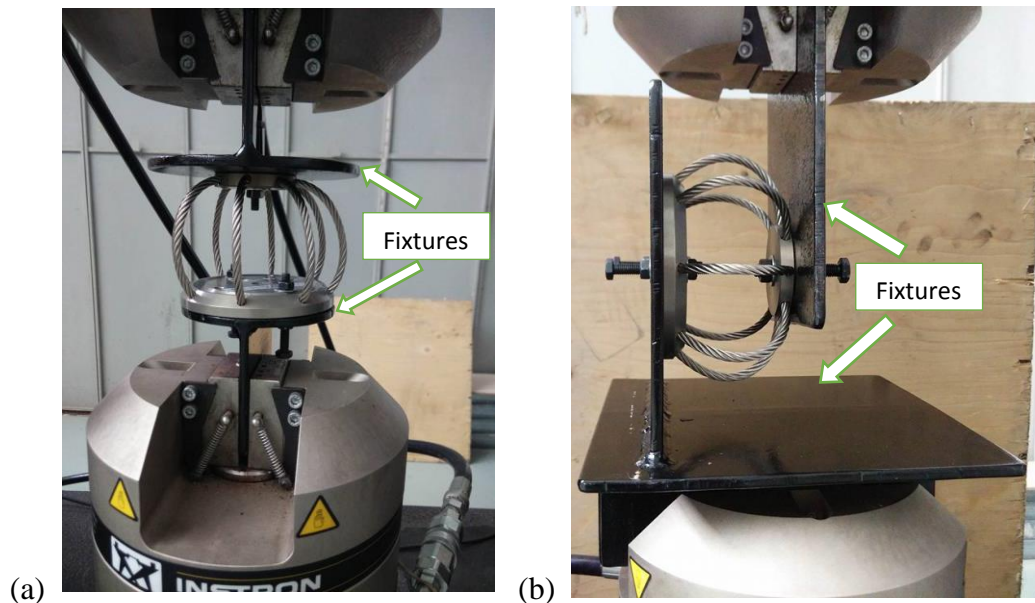


Figure 3.6 Fixtures used for the PWRI during loading test (a) Vertical fixtures (b) Lateral fixtures

3.6.4. Experimental procedure

The isolator was attached to fixtures using bolts and nuts. The fixtures were then secured to the UTTM through the UTTM clamping device. The monotonic compressive loading method and the displacement control settings were selected in the Bluehill Software. The test was configured to compress loading isolators up to 3mm

and then return to its original position (unloading). The isolators were controlled at a slow displacement of 2mm per minute, which was assumed to be quasistatic loading. Before a test began, a “RESET ALL” command was used to reset the initial loading and displacement value to zero, and was then followed by using the “START” command. The UTTM continuously recorded the load applied for every individual displacement made. After completion of each test, the test results were saved as a PDF (load-displacement graph) and as an excel file (datasheet). Before removing the isolators from the UTTM, the “RETURN” command should be used to return the displacement to the neutral position. Each test will be repeated three times and average result will be calculated. The same procedure was then repeated for the lateral loading but with a 1mm displacement.

3.7. Results

Vertical and lateral monotonic compression tests have been carried out and the results have been used to validate the analytical model represented by Equation 3.12 and Equation 3.20. Figure 3.7 shows the loading and unloading curve which was generated by the UTTM after the monotonic test. The initial loading and initial unloading stiffness was represented by K_1 while the final loading and final unloading stiffness was represented by K_2 (Weimin et al., 1997). Since the two springs constants K_1 and K_2 are connected in a series, the total stiffness K_v is given by,

$$\frac{1}{K_v} = \frac{1}{K_1} + \frac{1}{K_2} \quad (3.21)$$

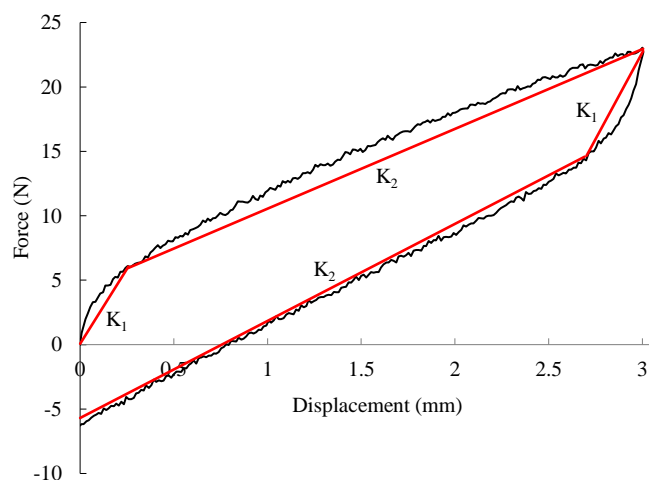


Figure 3.7 The double-linear retarding model of the PWRI

The comparison between the analytical and the experimental results of the vertical and lateral stiffness are tabulated in Table 3.2 and Table 3.3, respectively. From the comparison, we can conclude the differences between the analytical and experimental results of both the vertical and lateral stiffness's are similar, which shows a good agreement between them. The possible reason of the difference between analytical and experimental can be due to the specimens are having lower accuracy of dimension and some assumptions have been made as shown in section 3.3. The analytical models of the vertical and lateral stiffness are related to the geometric properties of the PWRI. The analytical study was carried out to investigate the influence of the number of wire rope strips, the wire rope diameter, and the radius of the curvature of the wire rope on the WRI's vertical and lateral stiffness. The mathematical model can be very useful in the design or modification of the PWRI to achieve the required stiffness or geometric properties. The PWRI is useful in many application such as function as stabilizer for camera which installed on the moving object.

Table 3.2 Comparison between analytical and experimental vertical stiffness of the PWRI

Isolator No.	Model	Experimental stiffness, K_v (N/mm)	Analytical stiffness, K_v (Eq. 3.12) (N/mm)
1	GGQ 1.0-37	14.2	15.4
2	GGQ 0.9-47	5.2	5.6
3	GGQ 0.55-56	3.1	3.1
4	GGQ 1.0-57	8.9	8.9
5	GGQ 1.7-71	3.8	4.0
6	GGQ 17-45	123.3	105.8
7	GGQ 15-62	36.2	26.8
8	GGQ 14-77	17.9	14.9
9	GGQ 29-71	85.4	61.0
10	GGQ 23-76	51.1	48.0

Table 3.3 Comparison of analytical and experimental lateral stiffness results

Isolator No.	Model	Experimental stiffness, K_L (N/mm)	Analytical stiffness, K_L (Eq. 3.20), N/mm
1	GGQ 1.0-37	5.0	7.7
2	GGQ 0.9-47	2.2	2.8
3	GGQ 0.55-56	1.5	1.5
4	GGQ 1.0-57	2.9	4.5
5	GGQ 1.7-71	1.6	2.0
6	GGQ 17-45	37.6	52.8
7	GGQ 15-62	12.5	13.4
8	GGQ 14-77	5.6	7.4
9	GGQ 29-71	24.8	30.4
10	GGQ 23-76	18.6	23.9

3.8. Parametric Analysis

In this section, a parametric analysis is performed to investigate the effects of different geometrical properties on the vertical compressive and lateral roll of WRIs stiffness. The parameters selected in this analysis are the wire rope diameter, the width and height of the isolator, and the number of wire rope strips.

3.8.1. Influence of wire rope diameter

The PWRI consists of a wire rope, which performs well in attenuating vibration. Thus, the stiffness of the PWRI depends on the wire rope characteristics. Figure 3.8 shows the influence of the wire rope diameter, D for a number of wire rope strips, N on vertical and lateral stiffness. Based on the analytical model, flexural rigidity is the main factor influencing stiffness. The flexural rigidity, EI of the wire rope is given by the equation, $EI = 39.72\phi^{3.97}$, which is determined by the diameter of the wire rope. Thus, an increase in diameter will eventually increase the vertical and lateral stiffness. Based on this equation, a diameter increase from 2.5mm to 6.4mm results in an increase in the stiffness by a factor of $(6.4/2.5)^{3.97} \approx 41.8$

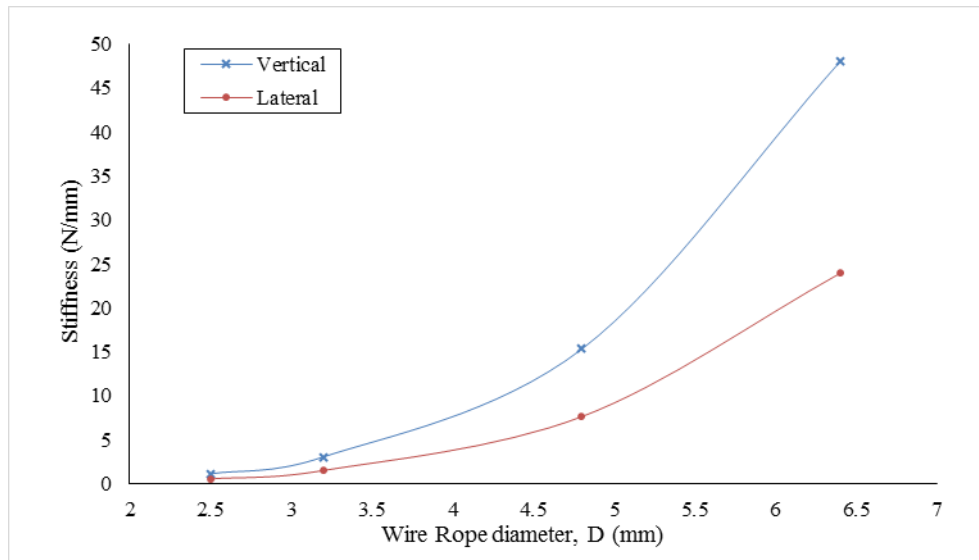


Figure 3.8 The influence of wire rope diameter, D and number of wire rope strip, $N = 8$ on vertical and lateral stiffness, with a constant radius of curvature, $R=38\text{mm}$

An increase in diameter will result in an increase in inertia of individual wires, which will then increase the resistance of the wire rope to lateral deformation (i.e., flexural rigidity, EI) and therefore resulting in a greater increase in vertical and lateral stiffness. The stiffness of the PWRI in the vertical direction is twice as stiff as in the lateral direction. The stiffness ratio can be defined using Equation (3.12) and Equation (3.20).

$$\frac{k_v}{k_L} \approx 2 \quad (3.22)$$

3.8.2. Influence of radius of curvature of wire rope, width, and height on the PWRI

The radius of curvature is one of the factors which directly affects the stiffness of the PWRI, which is influenced by its height and width. An increase in the radius of curvature, R , is governed by an increase in the height or a decrease in width, which results in the dramatic reduction of vertical and lateral stiffness as shown in Figure 3.9. Similar to Equation 3.12 and Equation 3.20, with the restricted parameters of the number of wire rope strips and wire rope diameter, the graph in Figure 3.9 can be said to have a cubically proportional relationship between stiffness and the radius of curvature. However, it should be noted that with an isolated parameter change such as

an increase in height or a decrease in width only, an increase of the height-to-width ratio would result which might then induce instability in the product from isolating lateral oscillations. As the restoring force is weakened in the horizontal direction, the reduction in overall performance of the isolator would arise. It should also be noted that if there was a reduction in the height-to-width ratio, more space in the horizontal direction would be consumed by the isolator, which might not be appropriate in situations where horizontal space is scarce. In addition, limitations may be imposed in the vertical and lateral displacement. Therefore, due to limitations of space, displacement, and stability, the height-to-width ratio was controlled to within the range of 0.41 to 0.74 as standardized by the manufacturer.

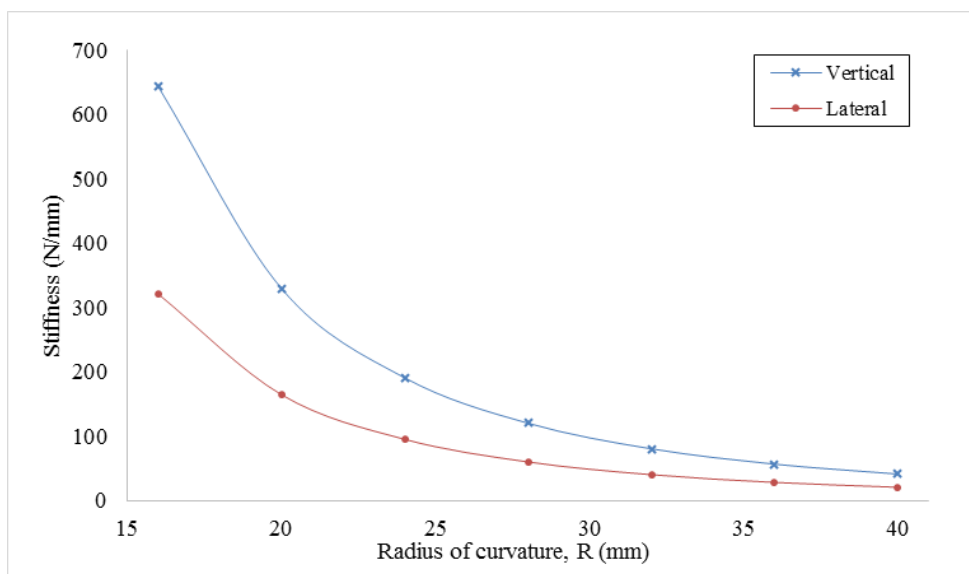
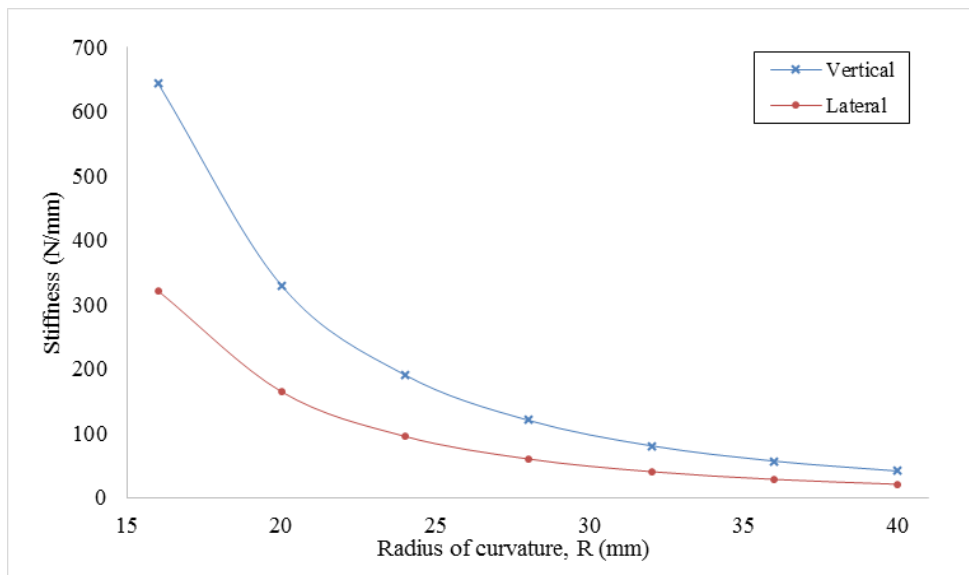


Figure 3.9 Influence of the radius of curvature on vertical and lateral stiffness with 8 numbers of wire rope strips and 6.4mm diameter of wire rope

3.8.3. Influence of the Number of wire rope strips

The number of wire rope strips is based on the weight of the supported equipment. Stiffness is directly proportional to the number of wire rope strips as determined by Equation 3.12 and Equation 3.20. Consequently, increasing the number of the wire rope strips will result in an increase in stiffness, as also shown in Figure 3.10. The greater the number of wire rope strips with smaller wire rope diameters will provide greater stability to the supported equipment compared to a lower number of wire rope strips with a larger wire rope diameter. By default, manufacturers manufacture the PWRI with eight wire rope strips to ensure greater stability.

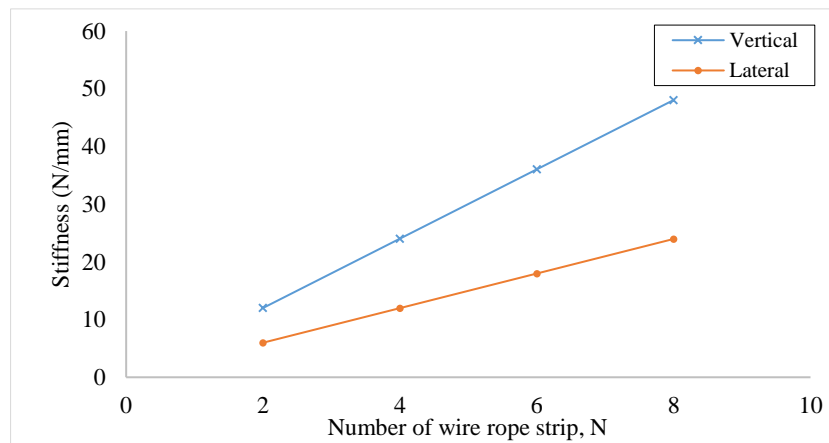


Figure 3.10 Influence of the number of wire rope strips on stiffness

3.9. Summary

An analytical model of the vertical and lateral stiffness of the PWRI has been developed in this study. Experimental data from the vertical and lateral monotonic tests were used to validate the developed analytical models. The analysis and design of the polycal wire rope isolators can be quite simple and effective with a well-developed model since the model relate the stiffness of PWRI to its geometrical properties. Parametric study was conducted and it enhance the understanding of the influence of the geometrical properties on the stiffness of PWRI. Several conclusions can be made from the study:

1. The vertical stiffness of the PWRI is approximately twice as stiff as in the lateral direction.
2. The PWRI stiffness is directly proportional to the number of wire rope strips.
3. The diameter of the wire rope has the greatest influence on stiffness compared to the radius of curvature, and the number of wire ropes.
4. Vertical and lateral stiffness increases with an increase in wire rope diameter but decreases with an increase in the radius of curvature of the PWRI.
5. An increase of 5% vertical and lateral stiffness can be achieved by reducing by 1.6% the radius of curvature of the wire rope or by increasing the wire rope diameter by 1.3%.

4. HYSTERESIS BEHAVIOUR OF PWRI

4.1. Introduction

This chapter presents the hysteresis behaviour of PWRI in vertical and lateral direction. The objective is to determine the hysteresis characteristics of the PWRI. Besides, investigation of the influences on the hysteresis characteristics are carried out.

4.2. Methodology

The cyclic loading tests were performed to study the hysteresis behaviour of PWRI. The PWRI with different geometric were subjected to vertical and lateral loadings. The hysteresis characteristics were presents as effective stiffness k_{eff} , energy loss ratio (ELR) and equivalent viscous damping ratio (EVDR) ζ_{eq} . The influence of different factors on the hysteresis characteristics were investigated such as rate test and height-width ratio. Same ten PWRI sample as chapter 3 were used in this study.

4.3. Experimental setup

Similar experimental setup as described for monotonic loading and unloading test in chapter 3, were used in cyclic loading. The slightly difference of cyclic loading was it consists of both positive and negative displacement to form a complete cycle. In this experiment, displacement was from origin to positive displacement in tension / upward, and then continues to negative displacement, which was in compression / downward and finally return to origin. This procedure was applied for 1mm, 2mm, and 3mm displacement amplitude. The rate is set to be slow rate, 8mm per minute to achieve quasi-static condition.

For rate test, Isolator 9 were chosen to perform cyclic loading test. Unlike the previous test using fixing rate, the rate test was conducted by using various loading rate which is 2mm/min, 4mm/min, 8mm/min, 16mm/min, 32mm/min, 64mm/min, and 128mm/min. The displacement amplitude was fixed at 6mm for the cyclic loading test. The test method command in Bluehill Software was configured to change loading rate after each complete cycle starting from 2mm/min to 128mm/min continuously.

4.3.1. Evaluation of Damping Characteristics

The effective stiffness, equivalent viscous damping ratio and energy loss ratio of the PWRI are determined from the results of cyclic loading by using Equation 4.1, Equation 4.4 and Equation 4.5 respectively (Balaji et al., 2015; Schwanen, 2004; Vaiana et al., 2017). Hysteresis curve is plotted based on the raw data obtained from the cyclic loading.

The effective stiffness is calculated by using the equation 4.1.

$$k_{eff} = \frac{F_{max} - F_{min}}{X_{max} - X_{min}} \quad (4.1)$$

where, X_{max} and X_{min} are the maximum and minimum displacements, respectively, F_{max} and F_{min} the maximum and minimum forces, respectively. The effective stiffness represent the overall stiffness of the full cycle motion. The stiffness is then used to calculate the restored elastic energy, E_s , which is

$$E_s = \frac{1}{2} k_{eff} X_{avg}^2 \quad (4.2)$$

Where X_{avg} is average of the maximum and minimum displacement values shown as

$$X_{avg} = \frac{X_{max} + X_{min}}{2} \quad (4.3)$$

The equivalent viscous damping ratio for hysteresis cycle is calculated using formula

$$\zeta_{eq} = \frac{E_d}{4\pi E_s} \quad (4.4)$$

Where E_d is the area within the hysteresis cycle. The area bounded by the hysteresis curve is calculated by using POLYAREA method of MATLAB software.

The Energy Loss Ratio (ELR) is calculated using the equation below.

$$ELR = \frac{E_d}{\pi \left(\frac{F_{max} - F_{min}}{2} \right) \left(\frac{X_{max} - X_{min}}{2} \right)} \quad (4.5)$$

4.4. Damping Characteristic of PWRI

The hysteresis behaviour of PWRI under cyclic loading with displacement amplitude of 1mm, 2mm and 3mm are discussed in this section since the hysteresis behaviour change with different displacement amplitudes. Besides, the energy loss ratio, effective stiffness and equivalent viscous damping ratio of the PWRI are determined using Equations 4.1 to Equation 4.5. The difference of the characteristics are displayed as chart and table and discussed in the following sections.

4.4.1. Hysteresis behaviour

The hysteresis behaviour analysed through the hysteresis curve under cyclic loading which represents the energy dissipation behaviour of the PWRI. The hysteresis curve consists of a complete loop of loading and unloading the isolator which involve positive displacement and negative displacement. The hysteresis curve is obtained through one complete loop of loading and unloading of the isolator, which involve positive and negative displacement. The energy dissipated by PWRI is represented by the area under the hysteresis curve due to the sliding friction between wire strands during cyclic loading condition.

4.4.1.1. *Hysteresis curve in vertical direction*

Figure 4.1, Figure 4.2 and Figure 4.3 show the hysteresis loops of PWRI under axial loading with 1mm, 2mm and 3mm displacement amplitudes respectively. Based on the observation from the figures, the hysteresis curves are asymmetric under tension and compression loading. It is harder to deform the isolators under tension loading if compared to compression loading with the same displacement amplitude. The phenomenon become more apparent at higher displacement amplitude. This phenomenon is caused by the hardening effect during tension loading while softening effect during compression loading. The wire strands become tense and stick closer to each other when the isolator is loaded under tension mode. Hence the friction increased between wire strands, the isolator become stiffer and higher load is required to pull the isolator. Conversely, the wire strands are become loose and move further away from

each other. Thus, the friction is reduced between wire strands, the isolators become less stiff and less load is required to compress the isolator.

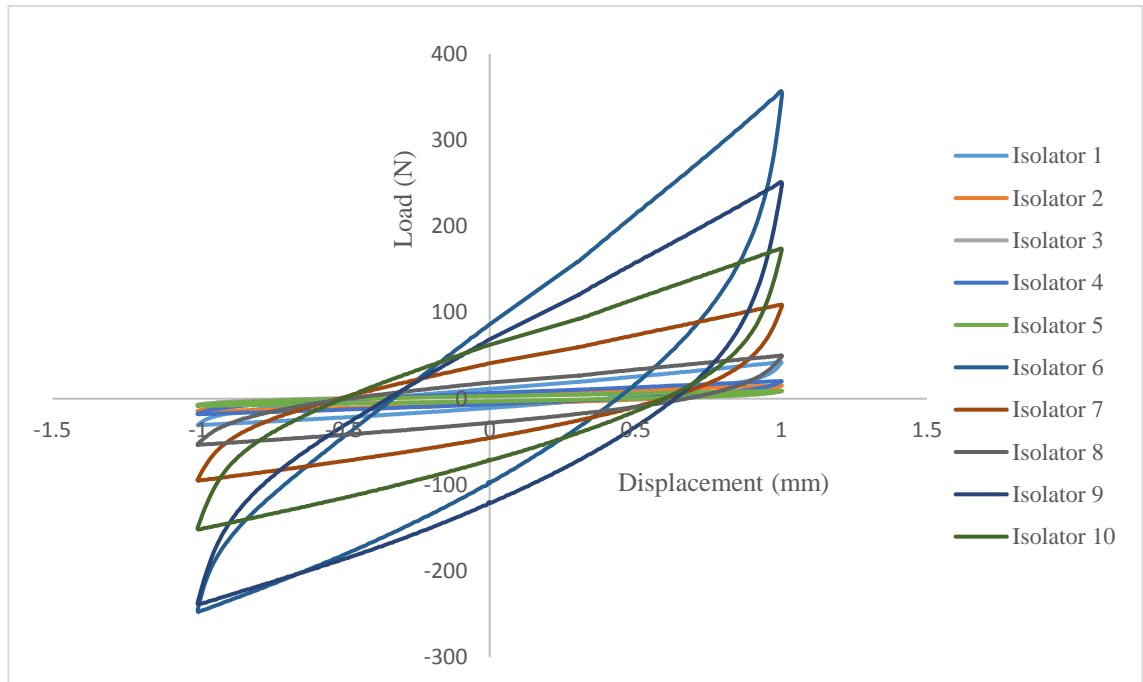


Figure 4.1 Hysteresis behaviour of isolators in vertical direction (1mm)

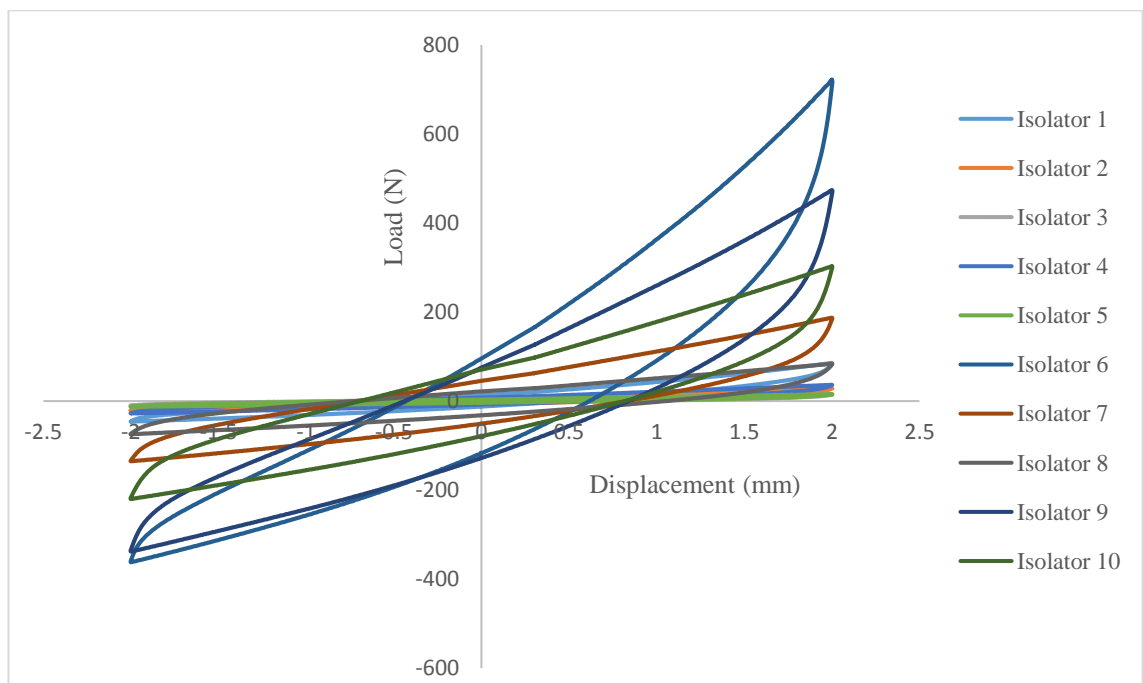


Figure 4.2 Hysteresis behaviour of isolators in vertical direction (2mm)

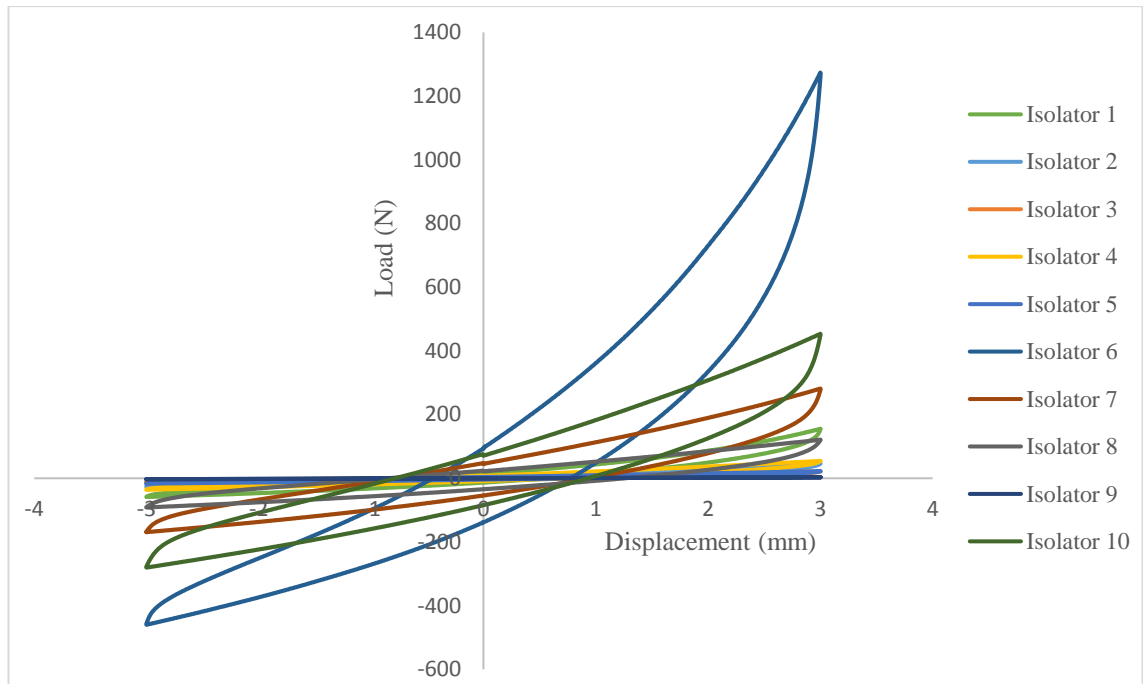


Figure 4.3 Hysteresis behaviour of isolators in vertical direction (3mm)

4.3.1.2 Hysteresis curve in lateral direction

The hysteresis curves of PWRI are acquired through displacing laterally the isolator with 1mm, 2mm and 3mm displacements respectively as shown in Figure 4.4, Figure 4.5 and Figure 4.6. The hysteresis curve of the PWRI under lateral loading is found to be different if compare to the hysteresis curve under vertical loading. The hysteresis curve appears to be almost symmetrical under lateral loading.

This phenomenon is due to the isolator exhibit hardening effect for both positive and negative direction loading. Since the isolator is symmetrical on the both sides of the isolators, the wire ropes are pulled and tightened in either direction, same total load are required to deform the isolator.

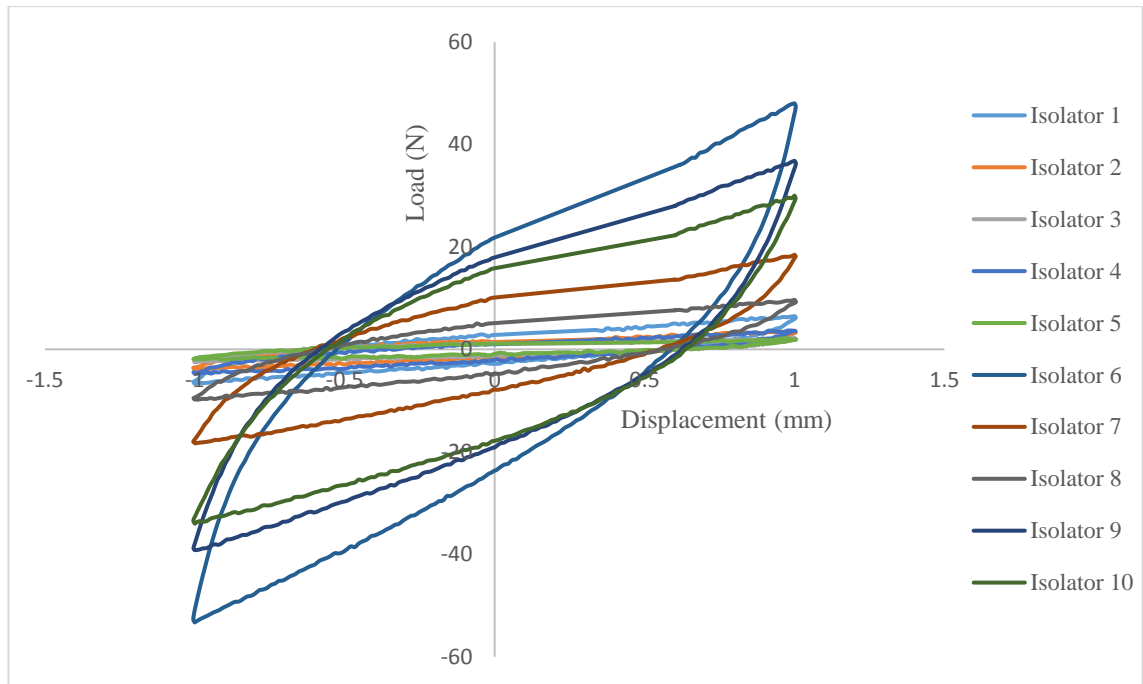


Figure 4.4 Hysteresis behaviour of isolators in Lateral Direction (1mm)

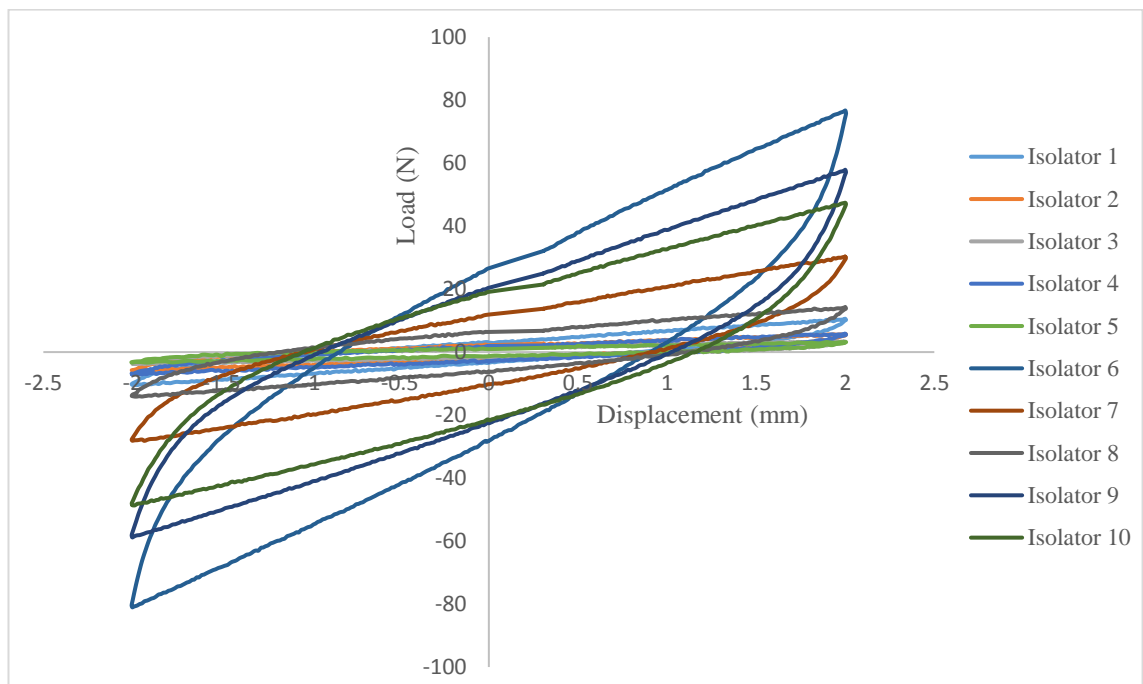


Figure 4.5 Hysteresis behaviour of isolators in Lateral Direction (2mm)

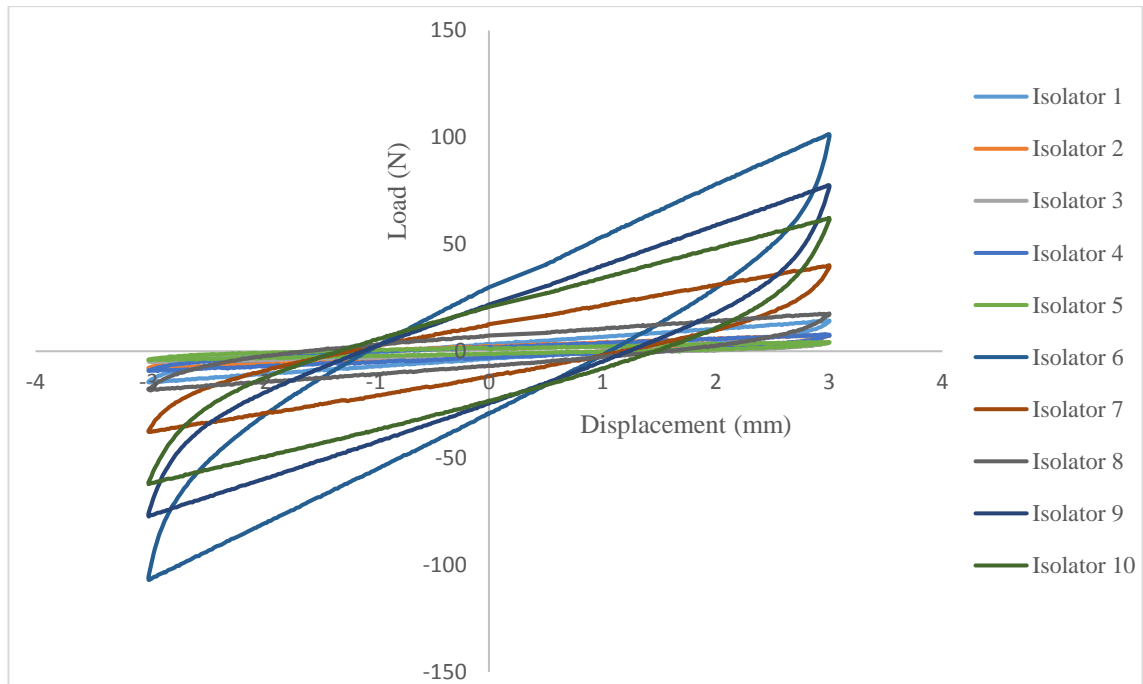


Figure 4.6 Hysteresis behaviour of isolators in Lateral Direction (3mm)

4.3.2 Energy loss ratio

Energy loss ratio (ELR) is used to determine the damping effectiveness of the PWRI. The ELR of the PWRI is the amount of dissipated energy with respect to viscous damping during cyclic loading. The higher ELR shows the better damping capability of PWRI. The ELR is determined from the hysteresis curves by applying Equation 4.5.

4.4.1.2. Energy Loss Ratio in Vertical Direction

Table 4.1 consists of the experimental data of the PWRI obtained from the vertical hysteresis curve. The ELR of the isolators are calculated based on the experiment data and the results are plotted as chart shown in Figure 4.7. For the 1mm displacement amplitude, the ELR for all isolators are in the range of 32% to 46%. When the displacement amplitude is increased to 2mm, the ELR of all isolators decreases. The ratios are in the range of 21.9% to 36.4% at this displacement amplitude. The ELR of the isolators further decrease to the range of 15.7% to 30% for the displacement amplitude of 3mm.

During displacement amplitude at 1mm, the isolators show the greatest values of ELR as shown in the ELR diagram. This indicates that all isolators have better damping effectiveness at lower displacement amplitude. The ELR decreases due to the decrease of the hysteresis curve area at the elevated displacement amplitude which indicate the poor damping effectiveness of the isolator.

Table 4.1 Experiment Data of Isolators from Hysteresis Curve (Vertical Direction)

No.	Isolator	Displacement amplitude (mm)	Hysteresis Loop Area (N.mm)	Max Force (N)	Min Force (N)	Max potential Energy	ELR (%)
1.	GGQ 1.0-37	1.0	38.16	42.57	-30.91	115.60	33.01
		2.0	90.80	85.59	-46.32	414.78	21.89
		3.0	158.36	155.20	-58.73	1,008.70	15.70
2.	GGQ 0.9-47	1.0	18.65	15.49	-14.56	47.32	39.41
		2.0	43.43	28.84	-20.92	156.51	27.75
		3.0	71.32	46.38	-26.29	342.72	20.81
3.	GGQ 0.55-56	1.0	10.81	8.88	-7.36	25.58	42.28
		2.0	26.32	14.81	-10.69	80.19	32.83
		3.0	43.64	21.76	-13.79	167.64	26.03
4.	GGQ 1.0-57	1.0	22.09	20.34	-17.95	60.29	36.64
		2.0	53.55	36.52	-27.68	201.93	26.52
		3.0	90.82	54.51	-36.10	427.33	21.25
5.	GGQ 1.7-71	1.0	10.39	9.27	-8.45	27.91	37.22
		2.0	25.04	15.42	-12.80	88.78	28.21
		3.0	41.57	22.35	-16.76	184.45	22.54
6.	GGQ 17-45	1.0	304.63	356.95	-247.54	951.95	32.00
		2.0	770.40	721.94	-362.17	3,410.02	22.59
		3.0	1420.10	1273.90	-459.93	8,177.03	17.37
7.	GGQ 15-62	1.0	142.73	109.17	-95.19	321.93	44.34
		2.0	329.00	187.42	-135.20	1,014.87	32.42
		3.0	537.28	281.73	-169.12	2,126.45	25.27
8.	GGQ 14-77	1.0	75.59	50.07	-53.94	163.82	46.14
		2.0	181.59	84.02	-74.44	498.53	36.42
		3.0	301.07	121.41	-91.57	1,004.62	29.97
9.	GGQ 29-71	1.0	312.79	251.48	-238.80	772.17	40.51
		2.0	713.31	474.14	-338.23	2,555.79	27.91
		3.0	1201.80	753.51	-429.17	5,578.79	21.54
10.	GGQ 23-76	1.0	222.93	174.23	-151.69	513.18	43.44
		2.0	521.41	303.55	-220.21	1,647.58	31.65
		3.0	867.43	453.76	-280.33	3,462.08	25.06

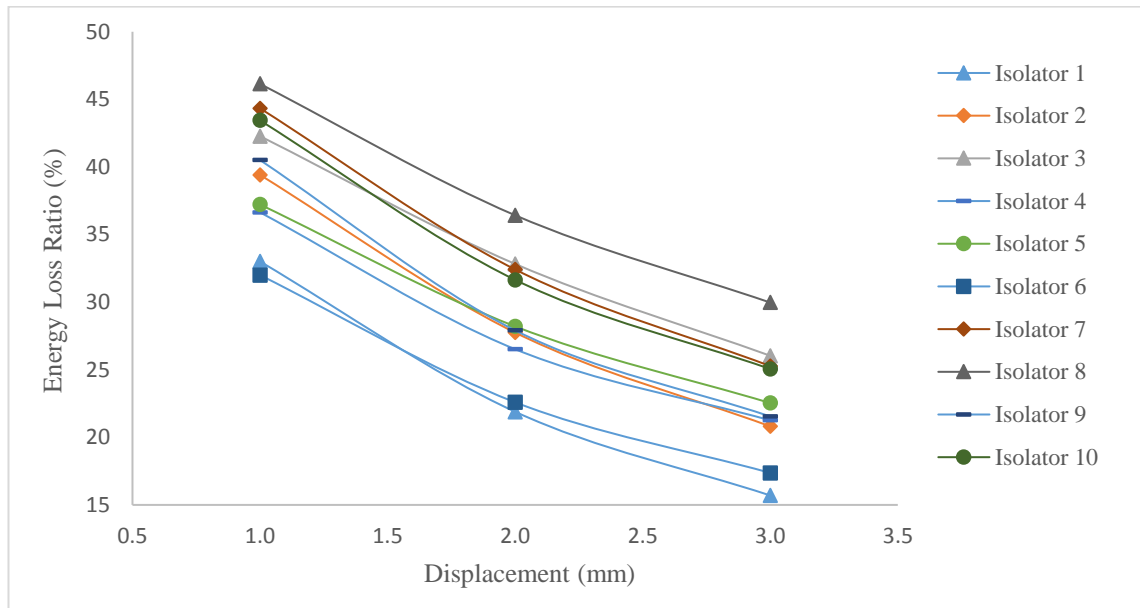


Figure 4.7 Energy Loss Ratio Diagram of Isolators (Vertical Direction)

4.4.1.3. Energy Loss Ratio in Lateral Direction

Table 4.2 shows the experimental data of the PWRI which extracted from the lateral hysteresis curve. Figure 4.8 depicted the changes of the ELRs of the PWRI based on the displacement amplitude. All the ELR of all isolators is within the range of 34% to 49.1% at the displacement amplitude of 1mm. When the displacement amplitude is increased to 2mm, the ELRs of all isolators decreases. The ratios are in the range of 33.5% to 44.9% at this displacement amplitude. The ERLs of the isolators further decrease for the displacement amplitude of 3mm. For the displacement amplitude of 3mm, the ELRs are in the range of 27% to 41.3%

The isolators have the similar behaviour which happened in vertical direction. At the lower displacement amplitude, all the isolators have the greatest values of ELR. This indicates that the PWRI has damping effectiveness at lower displacement amplitude.

Table 4.2 Experiment Data for ELR from Hysteresis Curve (Lateral Direction)

No.	Isolator	Displacement amplitude (mm)	Hysteresis Loop Area (N.mm)	Max Force (N)	Min Force (N)	Max potential Energy	ELR (%)
1.	GGQ 1.0-37	1.0	8.95	6.45	-6.71	20.67	43.28
		2.0	22.19	10.59	-10.48	66.20	33.52
		3.0	36.91	14.33	-14.64	136.53	27.04
2.	GGQ 0.9-47	1.0	5.25	3.64	-3.97	11.96	43.94
		2.0	13.85	5.65	-5.93	36.39	38.07
		3.0	23.29	7.65	-8.16	74.54	31.25
3.	GGQ 0.55-56	1.0	3.40	2.40	-3.97	10.00	34.03
		2.0	9.01	3.52	-3.81	23.04	39.11
		3.0	15.62	4.23	-5.06	43.78	35.67
4.	GGQ 1.0-57	1.0	5.05	3.66	-4.75	13.22	38.18
		2.0	14.40	5.85	-7.22	41.05	35.08
		3.0	25.05	7.99	-9.20	81.03	30.91
5.	GGQ 1.7-71	1.0	3.12	2.19	-2.01	6.60	47.28
		2.0	7.96	3.20	-3.34	20.55	38.75
		3.0	13.74	4.33	-4.21	40.24	34.16
6.	GGQ 17-45	1.0	71.21	48.02	-53.28	159.12	44.75
		2.0	178.52	76.73	-81.07	495.74	36.01
		3.0	296.85	101.55	-107.00	982.80	30.20
7.	GGQ 15-62	1.0	27.12	18.48	-18.36	57.86	46.87
		2.0	72.46	30.31	-28.19	183.78	39.43
		3.0	122.16	40.16	-37.76	367.16	33.27
8.	GGQ 14-77	1.0	14.56	9.68	-9.81	30.61	47.57
		2.0	40.16	14.33	-14.13	89.41	44.92
		3.0	69.90	17.59	-18.31	169.19	41.32
9.	GGQ 29-71	1.0	57.67	36.81	-39.19	119.37	48.31
		2.0	143.42	57.89	-58.86	366.78	39.10
		3.0	238.14	77.68	-77.31	730.40	32.60
10.	GGQ 23-76	1.0	49.42	30.01	-34.02	100.58	49.14
		2.0	130.52	47.43	-48.68	301.94	43.23
		3.0	219.47	62.32	-62.11	586.36	37.43

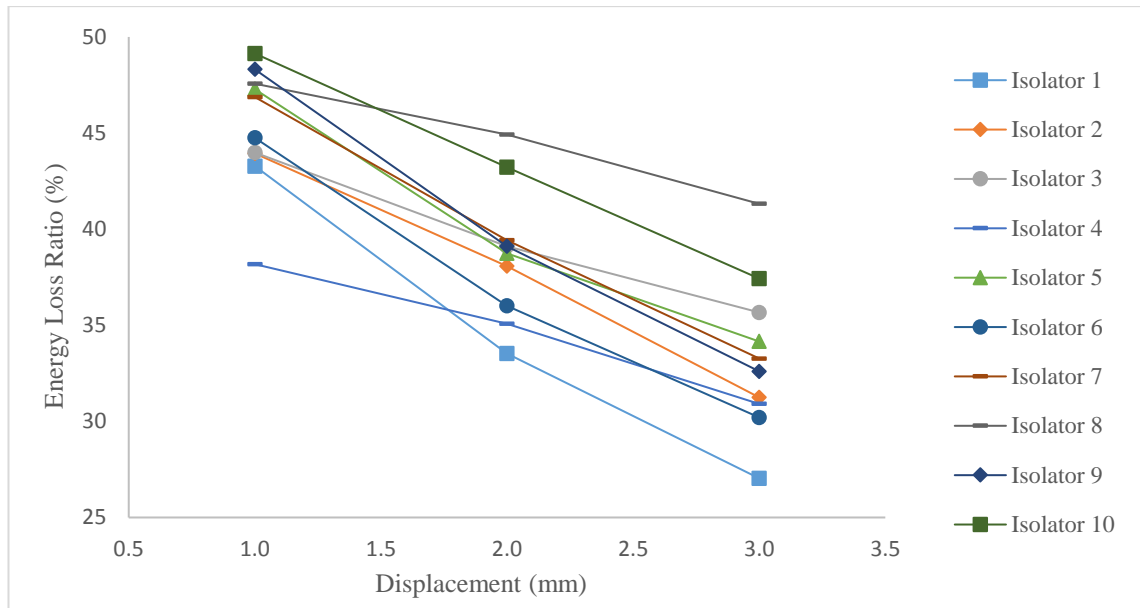


Figure 4.8 Energy Loss Ratio Diagram of Isolators (Lateral Direction)

4.4.2. Effective stiffness

The stiffness of the PWRI is changing when it is subjected to different magnitude of load. Therefore, the effective stiffness of the PWRI is determined to understand the stiffness variation due to the dynamic loading. The effective stiffness is calculated by dividing the value obtained from the difference between maximum force and minimum force with that obtained from the difference between maximum displacement and minimum displacement. It can be determined by using Equation 4.1.

4.4.2.1. Effective Stiffness in Vertical Direction

Table 4.3 summarizes the experimental data required for calculating the effective stiffness of PWRI in vertical direction. It can be observed from Figure 4.9 that the effective stiffness of PWRI changes with the geometrical properties. Isolator 6 has the highest effective stiffness while Isolator 3 has the lowest effective stiffness. The Isolator 6 possesses wire rope diameter of 4.8mm while the Isolator 3 is constructed with 2.5mm wire rope diameter. According to Balaji et al. (2015), the diameter of the wire rope is one the main contribution to the large difference of the effective stiffness.

To quantify the percentage of drop and rise of the effective stiffness with the increase in displacement amplitude, the effective stiffness was normalized with respect to the effective stiffness computed for 1 mm displacement amplitude of respective isolators. Figure 4.10 shows the normalized effective stiffness for different displacement amplitudes. All isolators have their highest effective stiffness when they are loaded under small displacement amplitude (1 mm).

The decrease of the effective stiffness at higher displacement amplitude is caused by the increase in the friction between the wire strands, resulting the decrease of moment of inertia of the isolator. According to Balaji et al. (2015), the effective stiffness will continue to decrease until the minimum value is reached and the effective stiffness starts to increase again. This phenomenon can be used to describe the increase of the effective stiffness of the isolators. The effective stiffness of the isolators has reached the minimum value at the displacement amplitude below the 1mm. Therefore, the decrease of the effective stiffness for these isolator is not observed from the test results. The increase in the effective stiffness following the minimum point is caused by the material hardening effect of the wire strand. In summary, the effective stiffness increases when the displacement amplitude increases.

Table 4.3 Experiment Data for Effective Stiffness from Hysteresis Curve (Vertical Direction)

No.	Isolator	Displacement amplitude (mm)	Max Force (N)	Min Force (N)	Effective Stiffness K_{eff} (N.mm)	Normalized Effective Stiffness (%)
1.	GGQ 1.0-37	1.0	42.57	-30.91	36.68	100.00
		2.0	85.59	-46.32	32.95	89.82
		3.0	155.20	-58.73	35.64	97.15
2.	GGQ 0.9-47	1.0	15.49	-14.56	14.98	100.00
		2.0	28.84	-20.92	12.42	82.91
		3.0	46.38	-26.29	12.10	80.76
3.	GGQ 0.55-56	1.0	8.88	-7.36	8.10	100.00
		2.0	14.81	-10.69	6.37	78.59
		3.0	21.76	-13.79	5.92	73.08
4.	GGQ 1.0-57	1.0	20.34	-17.95	19.10	100.00
		2.0	36.52	-27.68	16.03	83.94
		3.0	54.51	-36.10	15.09	79.00
5.	GGQ 1.7-71	1.0	9.27	-8.45	8.84	100.00

		2.0	15.42	-12.80	7.05	79.72
		3.0	22.35	-16.76	6.51	73.68
6.	GGQ 17-45	1.0	356.95	-247.54	301.48	100.00
		2.0	721.94	-362.17	270.69	89.79
		3.0	1273.90	-459.93	288.74	95.77
7.	GGQ 15-62	1.0	109.17	-95.19	101.90	100.00
		2.0	187.42	-135.20	80.55	79.05
		3.0	281.73	-169.12	75.08	73.68
8.	GGQ 14-77	1.0	50.07	-53.94	51.86	100.00
		2.0	84.02	-74.44	39.56	76.28
		3.0	121.41	-91.57	35.46	68.38
9.	GGQ 29-71	1.0	251.48	-238.80	244.49	100.00
		2.0	474.14	-338.23	202.80	82.95
		3.0	753.51	-429.17	196.92	80.54
10.	GGQ 23-76	1.0	174.23	-151.69	162.58	100.00
		2.0	303.55	-220.21	130.77	80.44
		3.0	453.76	-280.33	122.25	75.20

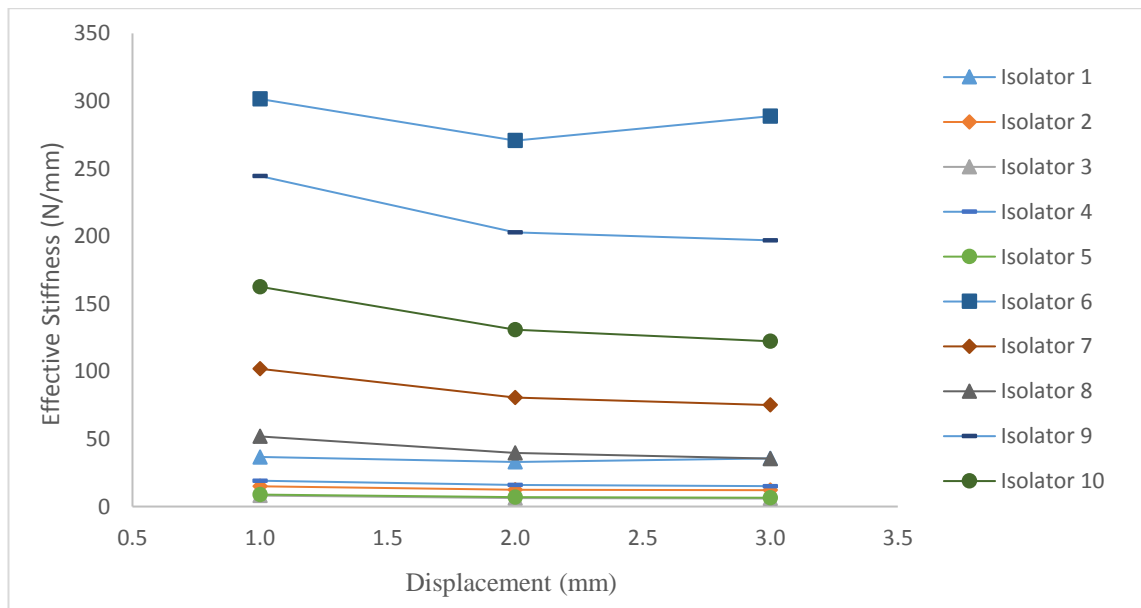


Figure 4.9 Effective Stiffness vs Displacement Amplitude (Vertical Direction)

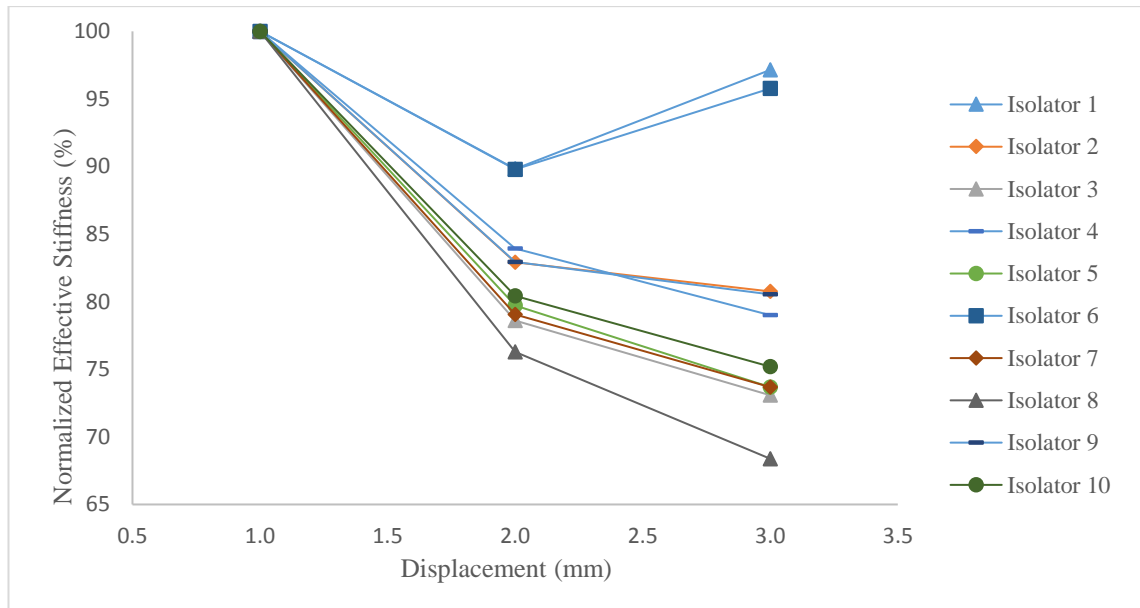


Figure 4.10 Normalized Effective Stiffness vs Displacement Amplitude (Vertical Direction)

4.4.2.2. Effective Stiffness in Lateral Direction

The experimental data for determining the effective stiffness in the lateral direction is tabulated in Table 4.4. Figure 4.11 depicts the change of effective stiffness of the PWRI with respect to the displacement amplitude. The Isolator 6 is the stiffest among the tested isolator while the Isolator 5 possesses the lowest effective stiffness. This is because the Isolator 6 is constructed with stiffer PWRI. The Isolator 6 has 4.8mm wire rope diameter of WRI. Meanwhile, the Isolator 3 is made up of 2.5mm wire rope diameter of WRI. Therefore, the Isolator 6 possesses the stiffer geometrical properties.

It is also found that the effective stiffness of the isolator in lateral direction is much smaller than the effective stiffness in vertical direction. Therefore, the PWRI is stiffer in vertical direction than the lateral shear direction. This has shown that the direction of applying has great influence on the effective stiffness and in this respect, the isolator is more effective in vertical direction.

The normalized effective stiffness of the isolator in lateral shear direction is shown in Figure 4.12. It is shown that the effective stiffness of all isolators decreases when the displacement amplitude increases. Besides, it can be observed that the effective stiffness of the isolators tend to decrease less at the higher displacement amplitude.

Table 4.4 Experiment Data for Effective Stiffness from Hysteresis Curve (Lateral Direction)

No.	Isolator	Displacement amplitude (mm)	Max Force (N)	Min Force (N)	Effective Stiffness K_{eff} (N.mm)	Normalized Effective Stiffness (%)
1.	GGQ 1.0-37	1.0	42.57	-30.91	6.58	100.00
		2.0	85.59	-46.32	5.27	80.06
		3.0	155.20	-58.73	4.83	73.38
2.	GGQ 0.9-47	1.0	15.49	-14.56	3.81	100.00
		2.0	28.84	-20.92	2.90	76.08
		3.0	46.38	-26.29	2.64	69.26
3.	GGQ 0.55-56	1.0	8.88	-7.36	2.46	100.00
		2.0	14.81	-10.69	1.83	74.44
		3.0	21.76	-13.79	1.55	62.87
4.	GGQ 1.0-57	1.0	20.34	-17.95	4.21	100.00
		2.0	36.52	-27.68	3.27	77.62
		3.0	54.51	-36.10	2.87	68.10
5.	GGQ 1.7-71	1.0	9.27	-8.45	2.10	100.00
		2.0	15.42	-12.80	1.63	77.88
		3.0	22.35	-16.76	1.42	67.79
6.	GGQ 17-45	1.0	356.95	-247.54	50.65	100.00
		2.0	721.94	-362.17	39.45	77.89
		3.0	1273.90	-459.93	34.76	68.63
7.	GGQ 15-62	1.0	109.17	-95.19	18.42	100.00
		2.0	187.42	-135.20	14.62	79.41
		3.0	281.73	-169.12	12.99	70.50
8.	GGQ 14-77	1.0	50.07	-53.94	9.74	100.00
		2.0	84.02	-74.44	7.11	73.01
		3.0	121.41	-91.57	5.98	61.41
9.	GGQ 29-71	1.0	251.48	-238.80	38.00	100.00
		2.0	474.14	-338.23	29.19	76.81
		3.0	753.51	-429.17	25.83	67.98
10.	GGQ 23-76	1.0	174.23	-151.69	32.02	100.00
		2.0	303.55	-220.21	24.03	75.05
		3.0	453.76	-280.33	20.74	64.78

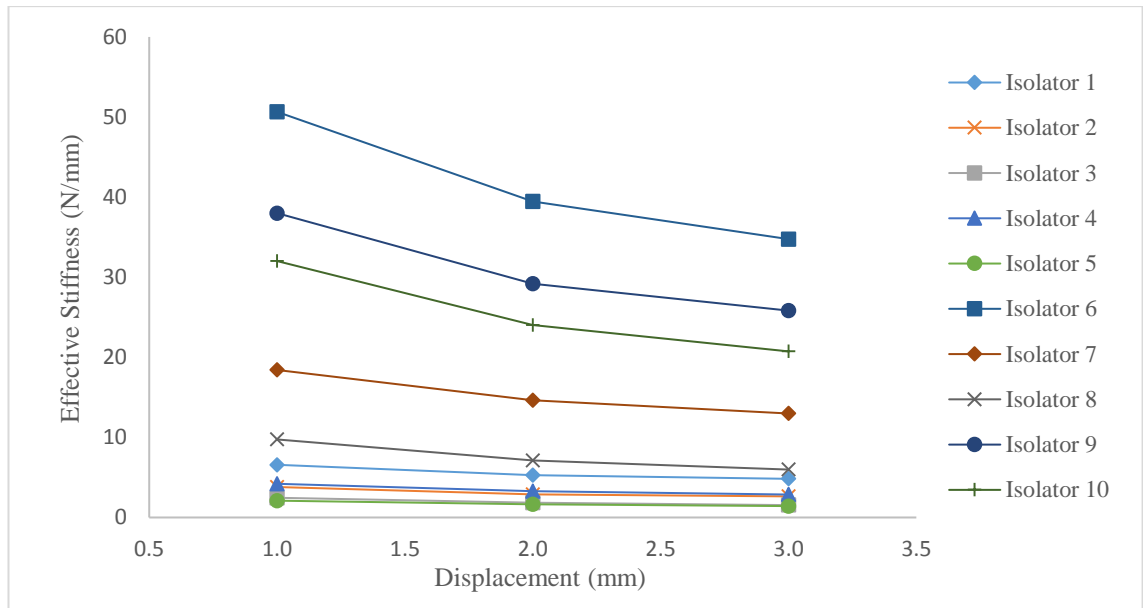


Figure 4.11 Effective Stiffness vs Displacement Amplitude (Lateral Direction)

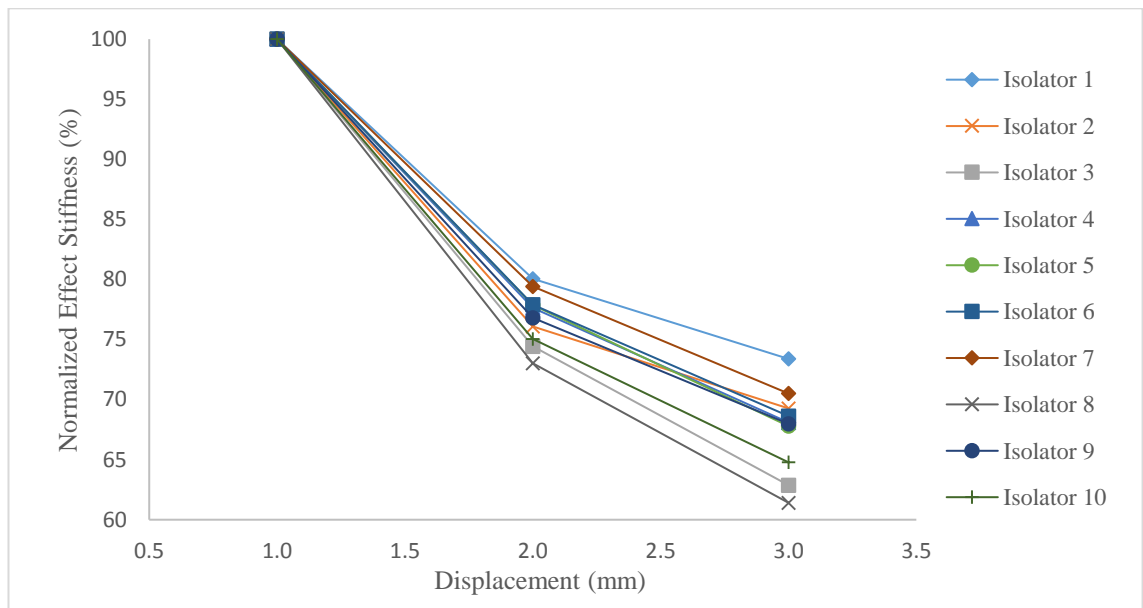


Figure 4.12 Normalized Effective Stiffness vs Displacement Amplitude (Lateral Direction)

4.4.3. Equivalent Viscous Damping Ratio (EVDR)

The EVDR of PWRI is determined to investigate the decaying of oscillation caused by vibration in the isolator. It is used to evaluate the energy dissipation capability of the isolator. The EVDR can be calculated by using Equation 4.4.

4.4.3.1. Equivalent Viscous Damping Ratio in Vertical Direction

Table 4.5 shows the calculated results of EVDR of PWRI in vertical direction. Figure 4.13 shows the EVDR of tested isolators for different displacement amplitude. For the 1mm displacement amplitude, the EVDR for all isolators are varies from 16% to 24%. For the 2mm displacement amplitude, the EVDR reduces for all isolators. The EVDR for all of the isolator during this displacement amplitude is from 10%-19%. For the 3mm displacement amplitude, the EVDR of all isolators further reduces. The EVDR range is from 7% to 15% in this displacement amplitude. From the observation of the diagram show in the Figure 4.13, the EVDR of the isolators reduces when the displacement amplitude increases, indicating the isolators are having less efficient damping characteristic. This is mainly due to that the wire rope strands move away from each other at higher displacement amplitude, reducing friction and also the damping effectiveness. The Isolator 1 has the lowest damping ratio while the Isolator 8 possesses the highest damping ratio among the tested isolators.

Table 4.5 Experiment Data for Equivalent Viscous Damping Ratio from Hysteresis Curve (Vertical Direction)

No.	Isolator	Displacement amplitude (mm)	Hysteresis Loop Area (N.mm)	Effective Stiffness, K_{eff}	Restored Elastic Energy, E_s	Equivalent Viscous Damping Ratio, ξ_{eq} (%)
1.	GGQ 1.0-37	1.0	38.16	36.68	18.34	16.56
		2.0	90.80	32.95	65.90	10.96
		3.0	158.36	35.64	160.36	7.86
2.	GGQ 0.9-47	1.0	18.65	14.98	7.49	19.81
		2.0	43.43	12.42	24.85	13.91
		3.0	71.32	12.10	54.45	10.42
3.	GGQ 0.55-56	1.0	10.81	8.10	4.05	21.25
		2.0	26.32	6.37	12.73	16.45
		3.0	43.64	5.92	26.63	13.04
4.	GGQ 1.0-57	1.0	22.09	19.10	9.55	18.41
		2.0	53.55	16.03	32.07	13.29
		3.0	90.82	15.09	67.90	10.64
5.	GGQ 1.7-71	1.0	10.39	8.84	4.42	18.71
		2.0	25.04	7.05	14.09	14.14
		3.0	41.57	6.51	29.31	11.29
6.	GGQ 17-45	1.0	304.63	301.48	150.74	16.08
		2.0	770.40	270.69	541.39	11.32

		3.0	1420.10	288.74	1,299.33	8.70
7.	GGQ 15-62	1.0	142.73	101.90	50.95	22.29
		2.0	329.00	80.55	161.10	16.25
		3.0	537.28	75.08	337.85	12.66
8.	GGQ 14-77	1.0	75.59	51.86	25.93	23.20
		2.0	181.59	39.56	79.12	18.26
		3.0	301.07	35.46	159.59	15.01
9.	GGQ 29-71	1.0	312.79	244.49	122.25	20.36
		2.0	713.31	202.80	405.61	13.99
		3.0	1201.80	196.92	886.12	10.79
10.	GGQ 23-76	1.0	222.93	162.58	81.29	21.82
		2.0	521.41	130.77	261.54	15.86
		3.0	867.43	122.25	550.13	12.55

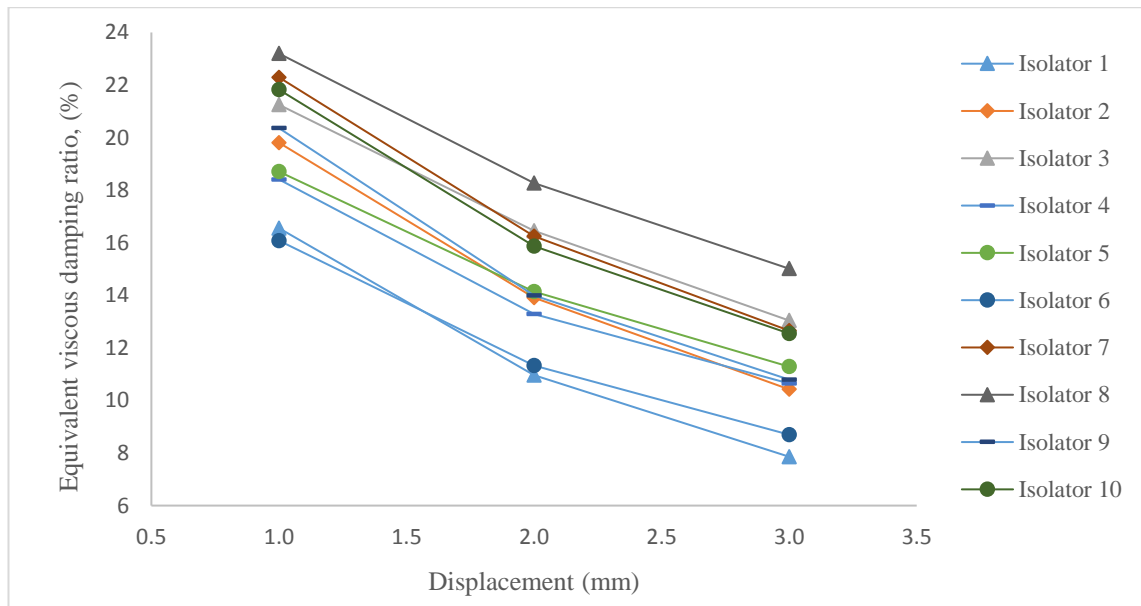


Figure 4.13 Equivalent Viscous Damping Ratio vs Displacement Amplitude (Vertical Direction)

4.4.3.2. Equivalent Viscous Damping Ratio in Lateral Direction

Table 4.6 shows the calculated results of EVDR of PWRI in vertical direction. Figure 4.14 shows the EVDR of tested isolators for different displacement amplitude. For the 1mm displacement amplitude, the EVDR is observed to be in the range of 19%-25%. For the 2mm displacement amplitude, the EVDR reduces for all isolators. The EVDR for all of the isolator during this displacement amplitude is from 16%-23%. For the 3mm displacement amplitude, the EVDR of all isolators further reduces. The EVDR

range is from 13% to 21% in this displacement amplitude. As an average result over three displacement amplitudes, the Isolator 1 possesses the lowest EVDR while the Isolator 8 has the highest EVDR. The EVDR of the tested isolators decreases when the displacement amplitude increases is due to the fact that the wire strands tend to move further apart at higher displacement amplitude. However, the EVDR of the isolators in lateral shear direction is higher than the vertical direction.

Table 4.6 Experiment Data for Equivalent Viscous Damping Ratio from Hysteresis Curve (Lateral Direction)

No.	Isolator	Displacement amplitude (mm)	Hysteresis Loop Area (N.mm)	Effective Stiffness, K_{eff}	Restored Elastic Energy, E_s	Equivalent Viscous Damping Ratio, ξ_{eq} (%)
1.	GGQ 1.0-37	1.0	8.95	6.58	3.29	21.64
		2.0	22.19	5.27	10.54	16.76
		3.0	36.91	4.83	21.73	13.52
2.	GGQ 0.9-47	1.0	5.25	3.81	1.90	21.97
		2.0	13.85	2.90	5.79	19.04
		3.0	23.29	2.64	11.86	15.62
3.	GGQ 0.55-56	1.0	3.40	2.46	1.23	21.99
		2.0	9.01	1.83	3.67	19.55
		3.0	15.62	1.55	6.97	17.83
4.	GGQ 1.0-57	1.0	5.05	4.21	2.10	19.09
		2.0	14.40	3.27	6.53	17.54
		3.0	25.05	2.87	12.90	15.45
5.	GGQ 1.7-71	1.0	3.12	2.10	1.05	23.64
		2.0	7.96	1.63	3.27	19.38
		3.0	13.74	1.42	6.40	17.08
6.	GGQ 17-45	1.0	71.21	50.65	25.32	22.38
		2.0	178.52	39.45	78.90	18.01
		3.0	296.85	34.76	156.42	15.10
7.	GGQ 15-62	1.0	27.12	18.42	9.21	23.44
		2.0	72.46	14.62	29.25	19.71
		3.0	122.16	12.99	58.44	16.64
8.	GGQ 14-77	1.0	14.56	9.74	4.87	23.78
		2.0	40.16	7.11	14.23	22.46
		3.0	69.90	5.98	26.93	20.66
9.	GGQ 29-71	1.0	57.67	38.00	19.00	24.16
		2.0	143.42	29.19	58.37	19.55

		3.0	238.14	25.83	116.25	16.30
10.	GGQ 23-76	1.0	49.42	32.02	16.01	24.57
		2.0	130.52	24.03	48.06	21.61
		3.0	219.47	20.74	93.32	18.71

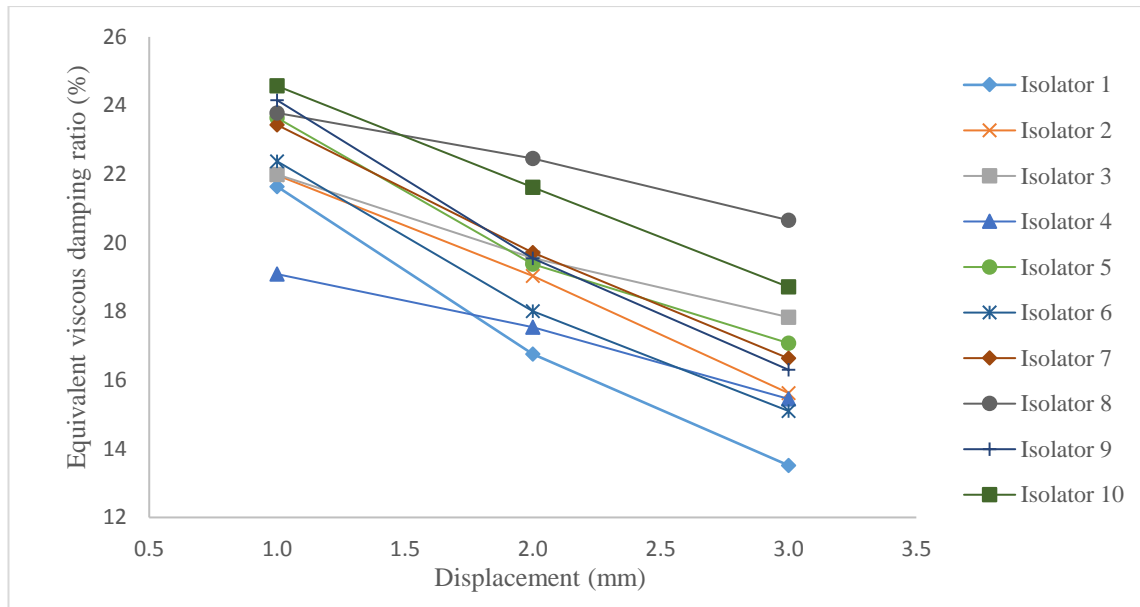


Figure 4.14 Equivalent Viscous Damping Ratio vs Displacement Amplitude (Lateral Direction)

4.5. Influence of Loading frequency

The loading speed were conducted at 2, 4, 8, 16, 32, 64, 128mm/min to determine the influence of the frequency on the hysteresis behaviour. From the Figures, it can be observed that all the hysteresis loops at different loading speed having similar position, which will result in similar hysteresis parameter. Besides, different wire rope diameter is also giving similar observation. Hence, it can be concluded PWRI will not be influenced by frequency.

The rate tests were conducted to determine the effects of variable frequency on the hysteresis behaviour of PWRI. From Figure 4.15 and Figure 4.16, the hysteresis loops were almost maintained in the same position with the varying loading rates and eventually formed a repeating same hysteresis loops. Thus, it is concluded that the behaviour of hysteresis exhibits rate independent memory effect as it is not dependent on the frequency of the applied load. The rate independence can be explained by the

dissipation phenomenon in hysteresis nature which is related to the sliding friction between wires.

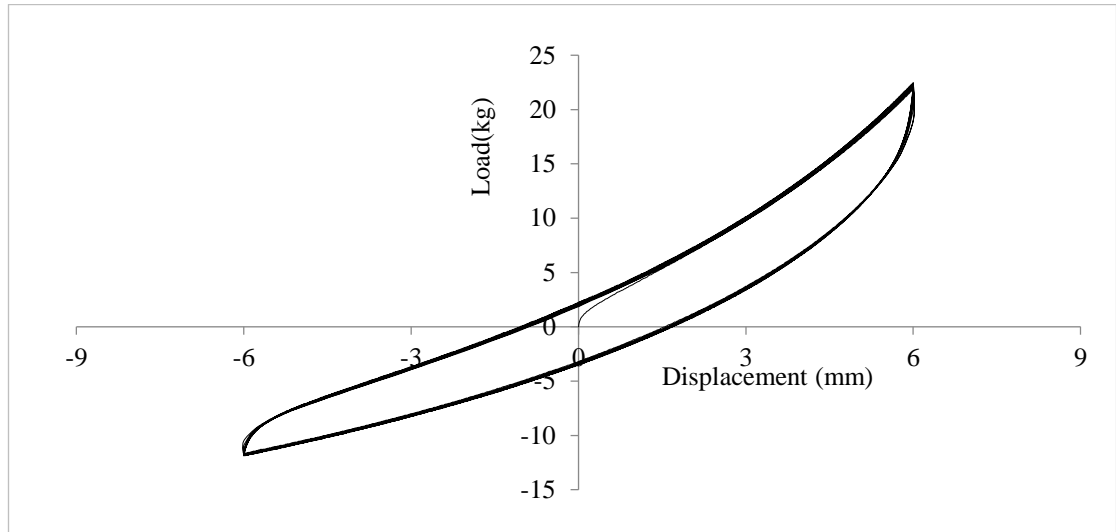


Figure 4.15 Rate Test for isolator 9 in tension/compression (wire rope diameter = 4.8mm)

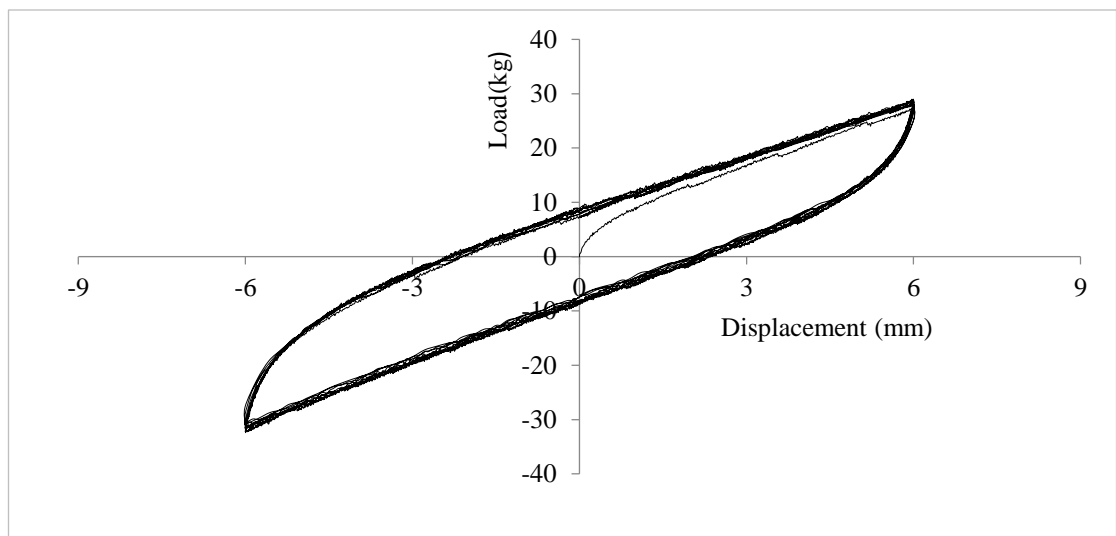


Figure 4.16 Rate Test for isolator 9 in lateral mode (wire rope diameter = 4.8mm)

4.6. Influence of height-to-width ratio of PWRI

Influence of height and width ratio are discussed in this section. The variations of energy loss ratio, effective stiffness and damping ratio for different displacements are

included to show the influence of displacement amplitude on the damping characteristics of PWRI. Figure 4.17 to Figure 4.22 show damping characteristics results of three isolators having the same wire rope diameter, 2.5mm but different height to width ratio, tested under 1mm, 2mm and 3mm loading displacement in vertical and lateral directions.

Figure 4.17 and Figure 4.18 show that the energy loss ratio is influenced by the height-to-width ratio. The energy loss ratio is increased when the height-to-width ratio increase in both vertical and lateral directions in all displacements.

Figure 4.19 and Figure 4.20 demonstrate that the effective stiffness is highly affected by the height-to-width ratio. The effective stiffness decrease when the height-to-width ratio increase for all displacement in vertical and lateral directions. The different become more obvious when in higher displacement which can be seen in Isolator 1 if compared to other isolators especially in vertical direction.

Figure 4.21 and Figure 4.22 show that the EVDR is influenced by the height-to-width ratio. The EVDR is increased when the height-to-width ratio increase in both vertical and lateral directions in all displacements.

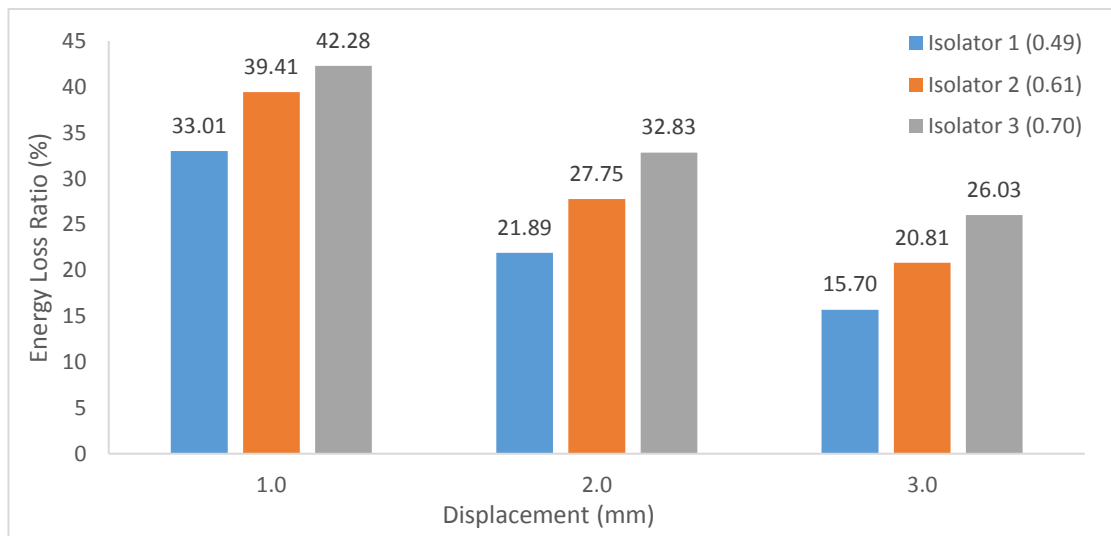


Figure 4.17 Variation of Energy Loss Ratio with height-to-width ratio in vertical direction

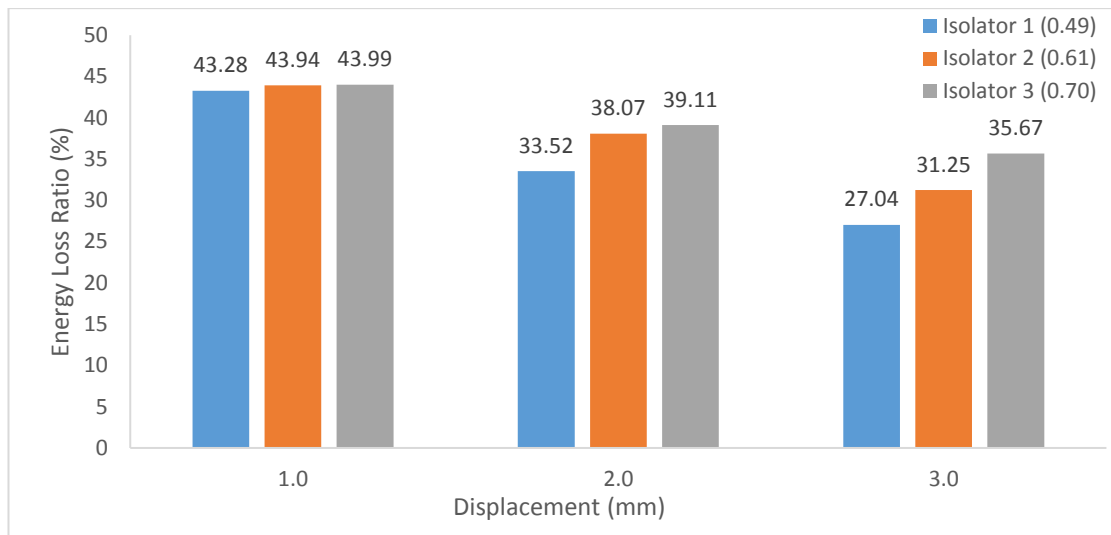


Figure 4.18 Variation of Energy Loss Ratio with height-to-width ratio in lateral direction

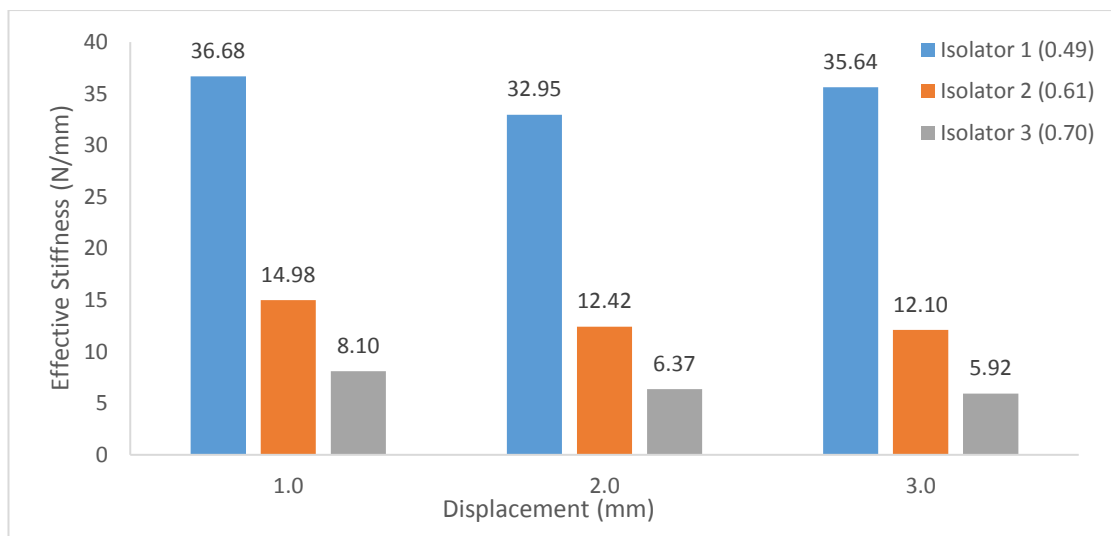


Figure 4.19 Variation of Effective Stiffness with height-to-width ratio in vertical direction

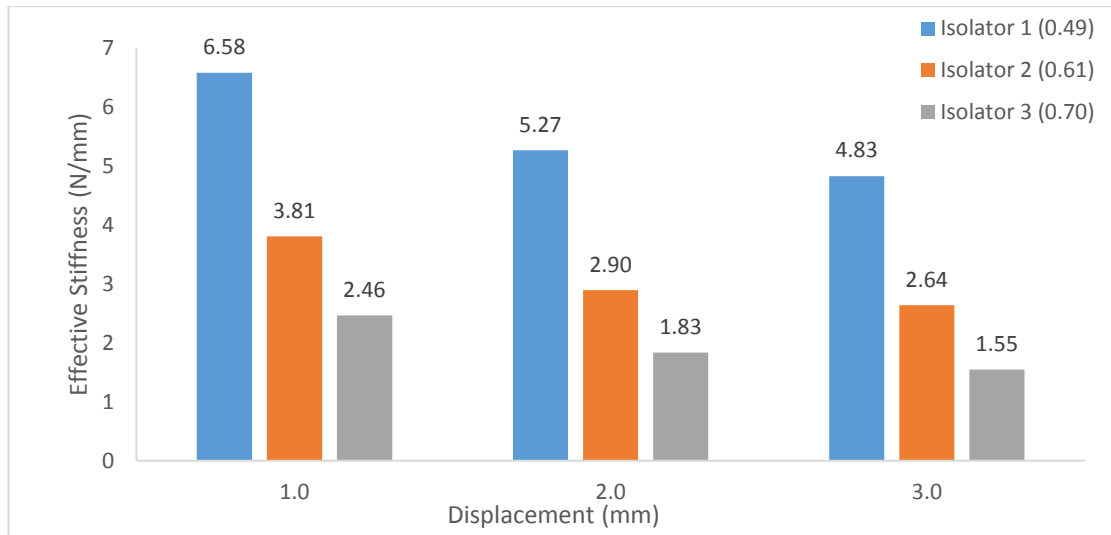


Figure 4.20 Variation of Effective Stiffness with height-to-width ratio in lateral direction

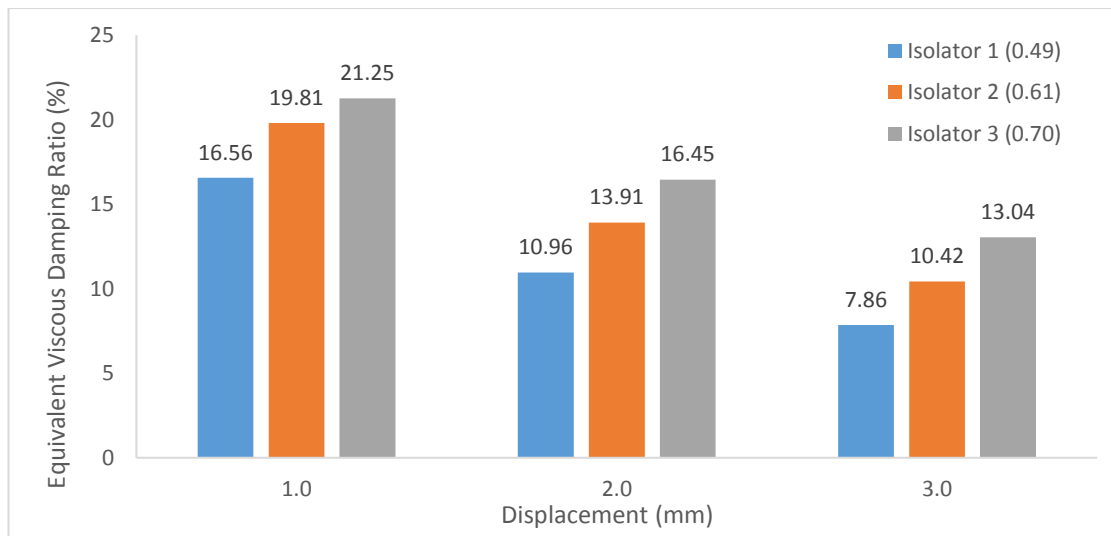


Figure 4.21 Variation of Equivalent Viscous Damping Ratio with height-to-width ratio in vertical direction

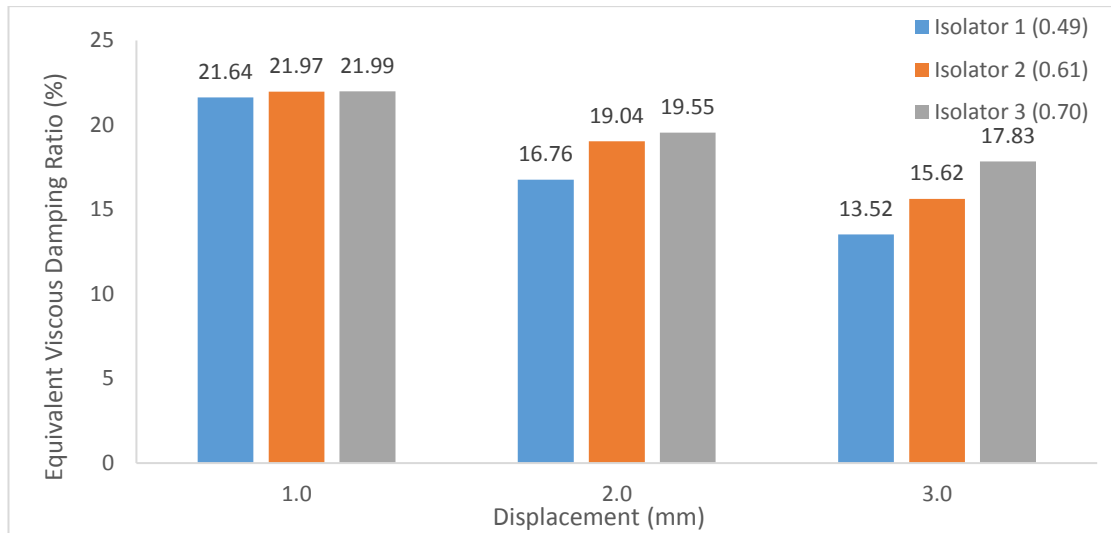


Figure 4.22 Variation of Equivalent Viscous Damping Ratio with height-to-width ratio in lateral direction

4.7. Summary

The hysteresis behaviour of the PWRI is evaluated by conducting the cyclic loading test in both vertical and horizontal directions. The damping characteristics of the isolators are examined by the factors of energy loss ratio, effective stiffness and damping ratio. It was found that the PWRI is rate independent in vertical and lateral directions. The hysteresis behaviour of PWRI will not be affected when loading rates vary. Besides, height-to-width ratio of PWRI affects the damping characteristics quite significantly. From the findings above, it is easy for designer to understand the behaviour of the PWRI. The findings provide important information to the designer such as the influence of the displacement amplitude on the damping characteristics of PWRI.

5. CONCLUSIONS AND RECOMMENDATIONS

5.1. Introduction

The research focuses on the study of vibration isolation ability of Polycal Wire Rope Isolator (PWRI) especially for industrial equipments. Two governing parameters of PWRI, namely stiffness and damping characteristics were evaluated throughout the research work. The stiffness is required by PWRI to support and provide stability to the equipment while the damping capability is needed for sufficient energy dissipation. In summary, nonlinear isolators such as PWRI is able to provide better isolation than linear isolators. Nevertheless, further study is still required to widen the potential areas of application of the PWRI in industrial sector. The following statements summarise and conclude the outcomes of this research project.

5.1.1. Objective 1

To establish a mathematical model of the stiffness of polycal wire rope isolators in both vertical and lateral directions and validate with the monotonic loading test results.

The stiffnesses of PWRI were evaluated through analytical and experimental works. The analytical models for stiffness in both vertical and lateral directions were developed by using Castigliano's second theorem. The models were then validated with the experimental results obtained from monotonic loading tests. It was found that the analytical results have a good agreement with the experimental results. The developed analytical models are crucial in providing convenience for the design and fabrication of PWRI in industry. Tedious and time-consuming experimental work for evaluating stiffness of PWRI can be avoided.

5.1.2. Objective 2

To investigate the damping characteristics of polycal wire rope isolators using cyclic loading conditions in both vertical and lateral directions.

The damping characteristics and hysteresis behaviour of PWRI in vertical and lateral directions were studied by performing a series of cyclic loading tests. Based on the experimental results, it has shown that the vertical hysteresis behaviour of PWRI is asymmetrical while the lateral hysteresis behaviour is symmetrical. Besides, it was also found that the PWRI is rate independent in vertical and lateral directions. The hysteresis behaviour of PWRI will not be affected when loading rates vary. Moreover, the PWRI experiences hardening under tensile force while it exhibits softening under compression. Lastly, it was shown that equivalent damping ratio of PWRI decreases when the displacement increases. Therefore, it is recommended to design the PWRI with having small displacements in order to ensure high efficiency of the isolator in energy dissipation.

5.1.3. Objective 3

To determine the effect of the wire rope's diameter, width and height on the stiffness using parametric study.

Parametric study was also performed on PWRI to study the effects of wire rope diameter, width and height on stiffness and damping characteristics. From the parametric study, it has shown that the PWRI in vertical direction is approximately two times stiffer than that in lateral direction. Also, the wire rope diameter of PWRI has greater influence on its vertical and lateral stiffness than other geometric properties such as number of wire rope strips and radius of curvature. Besides, the vertical and lateral stiffness of PWRI increases when the wire rope diameter increases. On the other hand, the stiffness decreases when the radius of curvature of PWRI decreases. For hysteresis behaviour, it was also found that increase in height-to-width ratio will result in the hardening of the PWRI. Increase in height-to-width ratio of PWRI will reduce the equivalent-damping ratio but greater energy are being dissipated. Thus, a PWRI with higher height-to-width ratio can be used when high-energy dissipation application is required. Lastly, the study has proven that the effective stiffness and damping ratio of PWRI significantly depend on the wire rope diameter. By adjusting the height-to-

width ratio of PWRI, a wide variety of effective stiffnesses and equivalent damping can also be obtained.

5.2. Recommendation for future work

It is required to discover wider field of application for PWRI that is more convenient and beneficial, particularly for industry. The following summarises the recommendation and improvement for future work.

1. For the present research work, the effect of wire rope diameter is not able to be studied due to the varying height and width of all isolators. Therefore, PWRI with varying wire rope diameter and constant height and width must be fabricated for further experimental investigation. As such, the parametric study can be performed to investigate the influence of wire rope diameter on damping characteristics in order to provide more insights regarding to the hysteresis behaviour of PWRI.
2. The mathematical model of the hysteresis behaviour of PWRI are recommended to developed in the future work.

REFERENCES

- AAC, Aroflex Isolators for Shock and Vibration. 2017.
<http://www.vibrationmounts.com>.
- Abolfathi, Ali. (2012). *Nonlinear Vibration Isolators with Asymmetric Stiffness*. (Doctor of Philosophy), UNIVERSITY OF SOUTHAMPTON, Southampton.
- Alanoly, James, & Sankar, Seshadri. (1987). A new concept in semi-active vibration isolation. *Journal of Mechanisms, Transmissions, and Automation in Design*, 109(2), 242-247.
- Balaji, P. S., Moussa, Leblouba, Rahman, M. E., & Ho, Lau Hieng. (2016). An analytical study on the static vertical stiffness of wire rope isolators. *Journal of Mechanical Science and Technology*, 30(1), 287-295. doi: 10.1007/s12206-015-1232-5
- Balaji, P. S., Moussa, Leblouba, Rahman, M. E., & Vuia, Loo Tshun. (2015). Experimental investigation on the hysteresis behavior of the wire rope isolators. *Journal of Mechanical Science and Technology*, 29(4), 1527-1536. doi: 10.1007/s12206-015-0325-5
- Balaji, Palani S., Leblouba, Moussa, Rahman, Muhammad E., & Ho, Lau Hieng. (2016). Static lateral stiffness of wire rope isolators. *Mechanics Based Design of Structures and Machines*, 44(4), 462-475. doi: 10.1080/15397734.2015.1116996
- Barry, O., Zu, J. W., & Oguamanam, D. C. D. (2015). Nonlinear Dynamics of Stockbridge Dampers. *Journal of Dynamic Systems, Measurement, and Control*, 137(6), 061017-061017. doi: 10.1115/1.4029526
- Barry, Oumar, Oguamanam, Donatus CD, & Lin, Der Chyan. (2013). Aeolian vibration of a single conductor with a Stockbridge damper. *Proceedings of the Institution of Mechanical Engineers, Part C: Journal of Mechanical Engineering Science*, 227(5), 935-945. doi: 10.1177/0954406212452064
- Chaudhuri, Sanjay, & Kushwaha, Bharat. (2008). Wire Rope Based Vibration Isolation Fixture For Road Transportation Of Heavy Defence Cargo. In E. İnan, D. Sengupta, M. Banerjee, B. Mukhopadhyay & H. Demiray (Eds.), *Vibration Problems ICOVP-2007* (Vol. 126, pp. 61-67): Springer Netherlands.

- Chiang, Young J. (1996). Characterizing simple-stranded wire cables under axial loading. *Finite elements in analysis and design*, 24(2), 49-66.
- Chungui, Zhou, Xinong, Zhang, Shilin, Xie, Tong, Zhou, & Changchun, Zhu. (2009). Hybrid modeling of wire cable vibration isolation system through neural network. *Mathematics and Computers in Simulation*, 79(10), 3160-3173. doi: 10.1016/j.matcom.2009.03.007
- Constantinou, Michalakis C, & Reinhorn, Andrei M. (1991). *Seismic Testing of Equipment Isolated by Wire-rope Isolators*: Department of Civil Engineering, State University of New York.
- Costello, G.A. (1997). *Theory of Wire Rope*: Springer New York.
- Costello, George A, & Butson, Gary J. (1982). Simplified bending theory for wire rope. *Journal of the Engineering Mechanics Division*, 108(2), 219-227.
- Demetriades, George F, Constantinou, Michalakis C, & Reinhorn, Andrei M. (1993). Study of wire rope systems for seismic protection of equipment in buildings. *Engineering structures*, 15(5), 321-334.
- Den Hartog, J.P. (1985). *Mechanical Vibrations*: Dover Publications.
- Di Massa, Giandomenico, Pagano, Stefano, Rocca, Ernesto, & Strano, Salvatore. (2013). Sensitive equipments on WRS-BTU isolators. *Meccanica*, 48(7), 1777-1790.
- Dominguez, A, Sedaghati, R, & Stiharu, I. (2008). Modeling and application of MR dampers in semi-adaptive structures. *Computers & structures*, 86(3), 407-415.
- Dong, Shufang, Lu, Ke-Qian, Sun, JQ, & Rudolph, Katherine. (2005). Rehabilitation device with variable resistance and intelligent control. *Medical engineering & physics*, 27(3), 249-255.
- DPFLEX. (2017a). GGT Series Wire Rope Isolator. *WUXI HONGYUAN DEVFLEX CO.LTD, China*.
- DPFLEX. (2017b). Shock & Vibration Control Wire rope Isolators. *WUXI HONGYUAN DEVFLEX Co. China*.
- Foss, Gary C. (2006). *Modal Damping Estimates from Static Load-Deflection Curves*. Paper presented at the 24th Conference and Exposition on Structural Dynamics 2006 (IMAC - XXIV), Missouri.
- Guyomar, D., Richard, C., & Mohammadi, S. (2008). Damping Behavior of Semi-passive Vibration Control using Shunted Piezoelectric Materials. *Journal of*

- Intelligent Material Systems and Structures*, 19(8), 977-985. doi: 10.1177/1045389x07083122
- Haberman, Michael R. (2007). *DESIGN OF HIGH LOSS VISCOELASTIC COMPOSITES THROUGH MICROMECHANICAL MODELING AND DECISION BASED MATERIALS DESIGN*. (Doctor of Philosophy), Georgia Institute of Technology, Georgia.
- Hobbs, RE, & Raoof, M. (1984). *Hysteresis in bridge strand*. Paper presented at the Institution of Civil Engineers, Proceedings, Pt2.
- Hoque, Md Emdadul, Mizuno, Takeshi, Kishita, Daisuke, Takasaki, Masaya, & Ishino, Yuji. (2010). Development of an active vibration isolation system using linearized zero-power control with weight support springs. *Journal of Vibration and Acoustics*, 132(4), 041006.
- Huang, Xiaolun, & Vinogradov, Oleg. (1994). Analysis of dry friction hysteresis in a cable under uniform bending. *Structural Engineering and Mechanics*, 2(1), 63-80.
- Huang, Xiaolun, & Vinogradov, Oleg G. (1996a). Dry friction losses in axially loaded cables. *Structural Engineering and Mechanics*, 4(3), 330.
- Huang, Xiaolun, & Vinogradov, Oleg G. (1996b). Extension of a cable in the presence of dry friction. *Structural Engineering and Mechanics*, 4(3), 313-329.
- Hunaidi, Osama. (2000). *Traffic vibrations in buildings*: Institute for Research in Construction, National Research Council of Canada.
- Ibrahim, RA. (2008). Recent advances in nonlinear passive vibration isolators. *Journal of sound and vibration*, 314(3), 371-452.
- Ismail, Mohammed, Ikhouane, Fayçal, & Rodellar, José. (2009). The hysteresis Bouc-Wen model, a survey. *Archives of Computational Methods in Engineering*, 16(2), 161-188.
- Jiang, WG, Yao, MS, & Walton, James M. (1999). A concise finite element model for simple straight wire rope strand. *International Journal of Mechanical Sciences*, 41(2), 143-161.
- Karnaikhov, VG, & Tkachenko, Ya V. (2011). Active damping of the resonant vibrations of a flexible cylindrical panel with sensors and actuators. *International Applied Mechanics*, 47(6), 720-726.

- Karnopp, Dean. (1995). Active and semi-active vibration isolation. *Journal of mechanical Design*, 117, 177-185.
- Klembczyk, Alan R. (2009). *Introduction to Shock and Vibration Isolation and Damping Systems*. Paper presented at the IMAC-XXVII: Conference & Exposition on Structural Dynamics.
- Leblouba, Moussa, Altoubat, Salah, Ekhlasur Rahman, Muhammad, & Palani Selvaraj, Balaji. (2015). Elliptical Leaf Spring Shock and Vibration Mounts with Enhanced Damping and Energy Dissipation Capabilities Using Lead Spring. *Shock and Vibration*, 2015, 12. doi: 10.1155/2015/482063
- Ledezma-Ramírez, Diego F, & Tapia-González, Pablo E. (2015). *Experimental characterisation of dry friction isolators for shock vibration isolation*. Paper presented at the Proceedings of the 22nd International Congress on Sound and Vibration. ISSN.
- Li, Gang, & Li, Hong-nan. (2009). *Pushover analysis method for asymmetric structure with passive energy dissipation devices*. Paper presented at the SPIE Smart Structures and Materials+ Nondestructive Evaluation and Health Monitoring.
- Li, Xiaoyong, Wang, Shilong, & Zhou, Jie. (2014). Analysis of elliptical Hertz contact of steel wires of stranded-wire helical spring. *Journal of Mechanical Science and Technology*, 28(7), 2797-2806.
- Loziuk, Larry A. (1988). A wire rope seismic support. *Nuclear Engineering and Design*, 107(1), 201-204. doi: [http://dx.doi.org/10.1016/0029-5493\(88\)90322-6](http://dx.doi.org/10.1016/0029-5493(88)90322-6)
- M.L. Tinker, M.A. Cutchins. (1989). Damping phenomena in a wire rope vibration isolation system, Doctor of Philosophy. *Aerospace Engineering, Auburn University*.
- Mallick, P. K. (1987). Static Mechanical Performance of Composite Elliptic Springs. *Journal of Engineering Materials and Technology*, 109(1), 22-26. doi: 10.1115/1.3225927
- Mallik, Asok Kumar. (1990). *Principles of vibration control*: Affiliated East-West Press.
- McCallion, H., & Davies, D. M. (1955). Behaviour of Rubber in Compression under Dynamic Conditions. *Proceedings of the Institution of Mechanical Engineers*, 169(1), 1125-1140. doi: 10.1243/pime_proc_1955_169_110_02

- Miller, B. A. (2004). Wire Ropes. In K. H. J. B. W. C. C. F. I. J. K. M. Veysière (Ed.), *Encyclopedia of Materials: Science and Technology (Second Edition)* (pp. 1-10). Oxford: Elsevier.
- Ni, Y Q, Ko, J M, Wong, C W, & Zhan, S. (1999). Modelling and identification of a wire-cable vibration isolator via a cyclic loading test. *Proceedings of the Institution of Mechanical Engineers, Part I: Journal of Systems and Control Engineering*, 213(3), 163-172. doi: 10.1243/0959651991540052
- Ni, YQ, Ko, JM, Wong, CW, & Zhan, S. (1999). Modelling and identification of a wire-cable vibration isolator via a cyclic loading test. *Proceedings of the Institution of Mechanical Engineers, Part I: Journal of Systems and Control Engineering*, 213(3), 163-172.
- Pagano, Stefano, & Strano, Salvatore. (2013). Wire rope springs for passive vibration control of a light steel structure. *WSEAS Transactions on Applied and Theoretical Mechanics*, 8(3), 212-221.
- Paolacci, F, & Giannini, R. (2008). *Study of the effectiveness of steel cable dampers for the seismic protection of electrical equipment*. Paper presented at the Proceedings of 14th World Conference on Earthquake Engineering.
- Platus, David L. (1992). Negative-stiffness-mechanism vibration isolation systems. *Vibration Control in Microelectronics, Optics, and Metrology, Proceedings OF SPIE*, 1619, 44-54.
- Preumont, André. (2002). *Vibration control of active structures: an introduction* (Vol. 179): Springer London, Limited.
- Raof, M. (1991). The prediction of axial damping in spiral strands. *The Journal of Strain Analysis for Engineering Design*, 26(4), 221-229.
- Raof, Mohammed. (1996). *Behaviour of large diameter wire ropes*. Paper presented at the The Fifth International Offshore and Polar Engineering Conference.
- Raof, Mohammed, & Davies, Timothy J. (2006). Simple determination of the maximum axial and torsional energy dissipation in large diameter spiral strands. *Computers & structures*, 84(10), 676-689.
- Rivin, E.I. (2003). *Passive Vibration Isolation*: ASME Press.
- Schwanen, W. (2004). Modelling and identification of the dynamic behavior of a wire rope spring. *Technische Universiteit Eindhoven*.

- Shaska, K., Ibrahim, R. A., & Gibson, R. F. (2007). Influence of excitation amplitude on the characteristics of nonlinear butyl rubber isolators. *Nonlinear Dynamics*, 47(1-3), 83-104. doi: 10.1007/s11071-006-9060-x
- Shigley, JE. (2008). Shigley's Mechanical Engineering Design, Vol. 8: McGraw-Hill, New York.
- Simmons, Robert. (2007). Vibration isolation. *ASHRAE*, 49, 30-40.
- Stanova, Eva, Fedorko, Gabriel, Fabian, Michal, & Kmet, Stanislav. (2011a). Computer modelling of wire strands and ropes Part I: Theory and computer implementation. *Advances in Engineering Software*, 42(6), 305-315.
- Stanova, Eva, Fedorko, Gabriel, Fabian, Michal, & Kmet, Stanislav. (2011b). Computer modelling of wire strands and ropes part II: Finite element-based applications. *Advances in Engineering Software*, 42(6), 322-331.
- Tanaka, N., & Kikushima, Y. (1989). On the Hybrid Vibration Isolation Method. *Journal of Vibration and Acoustics*, 111, 61-70.
- Tandon, I., Mallik, A. K., & Bhaya, P. Gupta. (1999). PERFORMANCE CHARACTERISTICS OF A VIBRATION ISOLATOR WITH ELECTRO-RHEOLOGICAL FLUIDS. *Journal of Sound and Vibration*, 219(3), 395-404. doi: <http://dx.doi.org/10.1006/jsvi.1998.1877>
- Tinker, Loyd, Michael, & Cutchins, Malcolm A. (1992). Damping phenomena in a wire rope vibration isolation system. *Journal of Sound and Vibration*, 157(1), 7-18.
- Tinker, M. L., & Cutchins, M. A. (1992). Damping phenomena in a wire rope vibration isolation system. *Journal of Sound and Vibration*, 157(1), 7-18. doi: [http://dx.doi.org/10.1016/0022-460X\(92\)90564-E](http://dx.doi.org/10.1016/0022-460X(92)90564-E)
- Tse, P. C., Lau, K. J., Wong, W. H., & Reid, S. R. (2002). Spring stiffnesses of composite circular springs with extended flat contact surfaces under unidirectional line-loading and surface-loading configurations. *Composite Structures*, 55(4), 367-386. doi: [http://dx.doi.org/10.1016/S0263-8223\(01\)00168-4](http://dx.doi.org/10.1016/S0263-8223(01)00168-4)
- Tse, PC, Lau, KJ, Wong, WH, & Reid, SR. (2002). Spring stiffnesses of composite circular springs with extended flat contact surfaces under unidirectional line-loading and surface-loading configurations. *Composite structures*, 55(4), 367-386.

- Vaiana, Nicolò, Spizzuoco, Mariacristina, & Serino, Giorgio. (2017). Wire rope isolators for seismically base-isolated lightweight structures: Experimental characterization and mathematical modeling. *Engineering Structures*, 140, 498-514.
- Velinsky, S. A. (1989). On the Design of Wire Rope. *Journal of Mechanisms, Transmissions, and Automation in Design*, 111(3), 382-388. doi: 10.1115/1.3259010
- Velinsky, Steven A. (1988). Design and mechanics of multi-lay wire strands. *ASME JOURNAL OF MECHANISMS, TRANSMISSIONS, AND AUTOMATION IN DESIGN*, 110(2), 152-160.
- Velinsky, Steven A. (1988). Design and Mechanics of Multi-Lay Wire Strands. *Journal of Mechanisms, Transmissions, and Automation in Design*, 110(2), 152-160. doi: 10.1115/1.3258920
- Velinsky, Steven A. (2004). Compressive Loading of Stiffened, Wire-Strand Based Structures. *Mechanics Based Design of Structures and Machines*, 32(1), 101-113. doi: 10.1081/SME-120026592
- Veprik, A. M., & Babitsky, V. I. (2000). VIBRATION PROTECTION OF SENSITIVE ELECTRONIC EQUIPMENT FROM HARSH HARMONIC VIBRATION. *Journal of Sound and Vibration*, 238(1), 19-30. doi: <http://dx.doi.org/10.1006/jsvi.2000.3098>
- Virgin, L. N., & Davis, R. B. (2003). Vibration isolation using buckled struts. *Journal of Sound and Vibration*, 260(5), 965-973. doi: [http://dx.doi.org/10.1016/S0022-460X\(02\)01177-X](http://dx.doi.org/10.1016/S0022-460X(02)01177-X)
- Wang, Hong-Xia, Gong, Xian-Sheng, Pan, Fei, & Dang, Xue-Jiang. (2015a). Experimental Investigations on the Dynamic Behaviour of O-Type Wire-Cable Vibration Isolators. *Shock and Vibration*, 2015, 12. doi: 10.1155/2015/869325
- Wang, Hong-Xia, Gong, Xian-Sheng, Pan, Fei, & Dang, Xue-Jiang. (2015b). Experimental investigations on the dynamic behaviour of O-type wire-cable vibration isolators. *Shock and Vibration*, 2015.
- Weimin, Chen, Gang, Liu, & Wei, Chen. (1997). Research on ring structure wire-rope isolators. *Journal of materials processing technology*, 72(1), 24-27.
- Winterflood, J., Barber, T. A., & Blair, D. G. (2002). Mathematical analysis of an Euler spring vibration isolator. *Physics Letters A*, 300(2-3), 131-139. doi: [http://dx.doi.org/10.1016/S0375-9601\(02\)00259-1](http://dx.doi.org/10.1016/S0375-9601(02)00259-1)

Winterflood, J., Blair, D. G., & Slagmolen, B. (2002a). High performance vibration isolation using springs in Euler column buckling mode. *Physics Letters A*, 300(2–3), 122-130. doi: [http://dx.doi.org/10.1016/S0375-9601\(02\)00258-X](http://dx.doi.org/10.1016/S0375-9601(02)00258-X)

Wire rope Isolators. (2016). *ITT EnidineInc, New York*.

Zhu, Z. H., & Meguid, S. A. (2007). Nonlinear FE-based investigation of flexural damping of slacking wire cables. *International Journal of Solids and Structures*, 44(16), 5122-5132. doi: <http://dx.doi.org/10.1016/j.ijsolstr.2006.12.024>

Every reasonable effort has been made to acknowledge the owners of copyright material. I would be pleased to hear from any copyright owner who has been omitted or incorrectly acknowledged.